

1 **Measurement report: Insights into the high temporal variability of**
2 **atmospheric carbon dioxide (CO₂) at a suburban station in the Indo-**
3 **Gangetic Plain**

4
5 Vimal Jose Vazhathara^{1, *}, Ravi Kumar Kunchala¹, Sajeev Philip¹, Jaswant Rathore¹, Dilip
6 Ganguly¹, Sagnik Dey^{1,2}, Yutaka Matsumi^{3,4} and Prabir K. Patra^{3,5}

7
8 ¹Centre for Atmospheric Sciences, Indian Institute of Technology Delhi, New Delhi, India.

9 ²Centre of Excellence for Research on Clean Air, Indian Institute of Technology Delhi, New
10 Delhi, India

11 ³Research Institute for Humanity and Nature, Kyoto, Japan

12 ⁴Institute for Space-Earth Environmental Research, Nagoya University, Nagoya, Japan

13 ⁵Japan Agency for Marine-Earth Science and Technology (JAMSTEC), Yokohama, Japan.

14 *Correspondence to: Vimal Jose Vazhathara (vimaljosevazhathara@gmail.com), Centre for
15 Atmospheric Sciences, Indian Institute of Technology Delhi, New Delhi, 110016, India

16
17 **Abstract**

18 The unusual weather patterns and large anthropogenic emissions over the Indo-Gangetic Plain
19 (IGP) make it a significant hotspot of greenhouse gases like carbon dioxide (CO₂). Given the
20 significance of the IGP, and highly populated Delhi National Capital Region (Delhi-NCR), a
21 GHG observatory was established at a suburban monitoring station in Sonipat, Haryana
22 (28.95°N, 77.10°E; 228m asl), about 45 km north of the Delhi state boundary. Using a laser-
23 based cavity ring-down spectroscopy (CRDS) technique, we measured CO₂ mole fraction from
24 February 2023 to January 2025. An annual average CO₂ mole fraction of 440.8±19.7 parts per
25 million (ppm) was recorded in 2024, which includes a strong seasonal variability, ranging from
26 422.6±23.3 ppm during the monsoon (June- September) to 456.4±30.8 ppm in post-
27 monsoon (October -November). A strong CO₂ diurnal amplitude of 29 ppm in May and 63 ppm
28 in October was observed mainly due to seasonal changes in boundary layer mixing (faster in

- Style Definition ... [8]
- Style Definition ... [7]
- Style Definition ... [6]
- Style Definition ... [5]
- Style Definition ... [4]
- Style Definition ... [3]
- Style Definition ... [2]
- Style Definition ... [1]
- Formatted ... [9]
- Deleted: paramount
- Formatted ... [10]
- Deleted: ,
- Formatted ... [11]
- Deleted: set up
- Formatted ... [12]
- Deleted: ,
- Formatted ... [13]
- Deleted:
- Formatted ... [14]
- Deleted:
- Deleted:), in
- Formatted ... [15]
- Formatted ... [16]
- Deleted: National Capital Region.
- Deleted: continuous measurements of CO₂ using
- Formatted ... [17]
- Formatted ... [18]
- Deleted: investigated the temporal evolution of
- Formatted ... [19]
- Deleted: We observed an
- Deleted: ±
- Formatted ... [20]
- Formatted ... [21]
- Formatted ... [22]
- Deleted: with an unusually
- Formatted ... [23]
- Formatted ... [24]
- Deleted: ±
- Deleted: ±
- Deleted: monsoon and
- Formatted ... [25]
- Formatted ... [26]
- Formatted ... [27]
- Formatted ... [28]
- Deleted: , respectively.
- Formatted ... [29]

46 May than October) and biospheric activity, (weaker in May than October). Further investigation
47 of the drivers of strong seasonal and diurnal CO₂ variability, over IGP revealed a strong contrast
48 to other global monitoring stations in the same latitude band. A strong correlation between CO₂
49 and methane (CH₄) indicated a co-located emission source, while the strong positive correlation
50 between CO₂ and carbon monoxide (CO) during post-monsoon emerges due to emissions from
51 biomass burning. We demonstrated that the high temporal CO₂ variability in the IGP region is
52 driven by the complex interplay of local anthropogenic and biomass burning emissions,
53 biospheric fluxes, and prevailing meteorology.

Deleted: .

Deleted: this unique feature (

Deleted:)

Deleted: indicates the footprint of crop residue

Deleted: on CO₂ mole fraction.

Deleted: demonstrate

54

55 1. Introduction

56 Carbon dioxide (CO₂) is the major greenhouse gas (GHG) contributing to climate change and
57 global warming (IPCC, 2021; Fawzy et al., 2020). Due to the long lifetime and high radiative
58 forcing potential, CO₂ can have a significant impact on global and regional climate (Wang et
59 al., 2010). The atmospheric CO₂ mole fraction, has increased from 278 parts per million (ppm)
60 in the pre-industrial period to 427 ppm in 2025 (NOAA, <https://gml.noaa.gov>; Wigley (1983).
61 This rapid increase in the atmospheric fraction of CO₂ is primarily due to the combustion of
62 fossil fuels, cement manufacture, deforestation, and other industrial processes (Stocker et al.,
63 2013; Huang et al., 2016; Yoro and Daramola, 2020). A comprehensive understanding of the
64 sources and sinks of CO₂ is critical for developing national policies to mitigate climate change
65 impacts.

Deleted: of CO₂

Deleted:).

66 India is the third-highest CO₂-emitting nation (8% of total global CO₂) in the last
67 decade, as reported by the Global Carbon Project (GCP) (Friedlingstein et al., 2025; Le Quéré
68 et al., 2018). In particular, the Indo-Gangetic Plain (IGP) region is one of the hotspots of
69 atmospheric CO₂ mole fraction, primarily due to large fossil fuel emissions and adverse
70 meteorology (Halder et al., 2021; Krishnapriya et al., 2025; Kuttippurath et al., 2022). Over the
71 past few decades, the IGP region has witnessed rapid urbanisation, industrialisation, and
72 agricultural intensification, leading to significant changes in land-use patterns and GHG
73 emissions (Yoro and Daramola, 2020). Mitigation of anthropogenic CO₂ emissions in the
74 highly populated IGP region is crucial to reducing the build-up of atmospheric CO₂ mole
75 fractions. Gaining a better understanding of the magnitude of CO₂ sources and sinks and the
76 local drivers of CO₂ temporal variability over the IGP region is therefore important.

Deleted:

Deleted:

Deleted: In particular, the Indo-Gangetic Plain (IGP) region is one of the hotspots for atmospheric CO₂ mole fraction primarily due to the large fossil fuel emissions and adverse meteorology (Kuttippurath et al., 2022; Singh et al., 2022).

Deleted: over

Deleted: for

Deleted: high

Deleted: fraction build-up

Deleted: The continuous monitoring of ground-based CO₂ is of utmost importance for the inverse modelling approaches to understand the sources and sinks of CO₂. Although GHG mole fraction have been monitored over various parts of the globe for decades, monitoring stations of GHGs in India are limited (Chakraborty et al., 2020; Kumar et al., 2021; Patra et al., 2013; Tiwari et al., 2013) The Cape Rama (15.08° N, 73.83° E), situated on India's southwest coast, was the first Indian monitoring station tracking

77

105 Continuous monitoring of ground-based CO₂ is of utmost importance for inverse
 106 modelling approaches to understand local-to-regional-scale sources and sinks of CO₂.
 107 Although GHG mole fractions have been monitored worldwide for decades, GHG monitoring
 108 stations in India are limited (Kunchala et al., 2025; Chakraborty et al., 2020; Kumar et al.,
 109 2021; Patra et al., 2013; Tiwari et al., 2013). The Cape Rama (15.08° N, 73.83° E) station,
 110 situated on India's southwest coast, was the first Indian monitoring station to track CO₂ mole
 111 fraction from 1993 to 2002 (Bhattacharya et al., 2009; Patra et al., 2011; Rayner et al., 2008).
 112 Recently, several monitoring stations have been established over different parts of India to
 113 measure the GHGs (Chandra et al., 2016; Jain et al., 2021; Mahesh et al., 2015; Metya et al.,
 114 2021; Nomura et al., 2021; Pathakoti et al., 2023; Sreenivas et al., 2016; Thilakan et al., 2023;
 115 Tiwari et al., 2014). Studies have also been conducted using aircraft-based measurements
 116 (Niwa et al., 2012; Patra et al., 2011; Schuck et al., 2012; Zhang et al., 2007) and satellite data
 117 products (Das et al., 2023; Kunchala et al., 2022; Nalini et al., 2019; Philip et al., 2022; Xiong
 118 et al., 2009). The incorporation of regional in situ and aircraft-based measurements, along with
 119 satellite columnar CO₂ retrievals, reduced uncertainties in top-down CO₂ flux estimates (Huang
 120 et al., 2008; Niwa et al., 2012; Zhang et al., 2014).

121 To comprehensively understand temporal CO₂ variability and its drivers in the western
 122 IGP region, we have conducted atmospheric CO₂ mole fraction measurements at Sonipat, a
 123 suburban station in the IGP region upwind of Delhi. The continuous measurements from
 124 February 2023 to January 2025 were conducted using laser-based cavity ring-down
 125 spectroscopy. Here, we investigate the novel characteristics of the seasonal and diurnal
 126 variability of atmospheric CO₂ mole fraction at Sonipat. We then identify the key drivers of
 127 the observed temporal CO₂ variability in the region.

129 2. Materials and methods

130 2.1 Monitoring station

131 The measurements in this study were carried out at the Indian Institute of Technology Delhi
 132 (IIT Delhi) Centre for Atmospheric Sciences (CAS) - Atmospheric Observatory situated at
 133 Sonipat campus (28.95°N, 77.10°E, 228m asl). Sonipat is an upwind suburban region of the
 134 Delhi-NCR, situated in the northern Indian state of Haryana, approximately 45 kilometres north
 135 of Delhi. The monitoring station is surrounded by agricultural fields, a National Highway, and
 136 academic institutions (Rathore et al., 2025). Figure 1 shows the location map of the monitoring
 137 station. The climatic conditions over this site are similar to Delhi which has sweltering
 138 summers (March-May), damp or moist monsoons (June - September), and extreme winters.

- Deleted: Some
- Deleted: -based
- Deleted: studies have also been conducted in the past.
- Deleted: the
- Deleted: column
- Deleted: estimations
- Deleted: These studies highlighted the importance of regional ground-based observations in constraining Indian carbon cycle dynamics. However, the IGP region still lacks continuous measurements to track temporal evolution of atmospheric CO₂ mole fraction except for one station in Mohali (Thilakan et al., 2023).
- Deleted: the
- Deleted: along with
- Deleted: magnitude and the
- Deleted: of CO₂
- Deleted: the
- Deleted: technique
- Deleted: over the
- Deleted: monitoring station.
- Deleted: over the Sonipat station to gain insights into the carbon cycle dynamics of the entire IGP
- Formatted: Font colour: Black
- Deleted: 95° N
- Deleted: 10° E, 228 m amsl altitude).
- Formatted: Font colour: Black
- Formatted: Font colour: Black
- Formatted: Font colour: Black
- Deleted: north
- Deleted: and a part
- Formatted: Font colour: Black
- Formatted: Font colour: Black
- Formatted: Font colour: Black
- Deleted: the
- Deleted: National Capital Region (NCR).
- Formatted: Font colour: Black
- Formatted: Font colour: Black
- Deleted: .
- Deleted: ,

169 Similar to Delhi, this region also has frequent haze and smog with low visibility during winter
170 (December - February) and post-monsoon (October - November) seasons. During the post-
171 monsoon season, Sonipat experiences large transport of pollutants from the North-West
172 direction. In addition to the pollutant transport, several local emission sources exist in the
173 region, such as small industries, vehicular sources, and local biomass burning affecting short-
174 lived air pollutants (Rathore et al., 2025).

Deleted: station

Deleted: emissions

Deleted: .

176 2.2 Local measurements

177 2.2.1 GHG measurements

178 This study utilised the PICARRO G2301 GHG analyser to measure major atmospheric GHG
179 mole fractions. The PICARRO analyser employs the Cavity Ring-Down Spectroscopy (CRDS)
180 technique at 0.5 Hz to measure CO₂ mole fraction. The CRDS technique utilises the ring-down
181 time of light intensity within the cavity to determine the mole fraction of CO₂, a method
182 fundamentally different from other measurement techniques such as Non-dispersive Infrared
183 Spectroscopy (NDIR) and Fourier Transform Infrared Spectroscopy (FTIR). The long sample
184 interaction path length (approximately 20 km) is a characteristic of CRDS, which enhances
185 sensitivity compared to conventional techniques based on light-intensity absorption. The cavity
186 pressure operates at a very low pressure of 140 Torr. This isolates a single spectral feature with
187 a resolution of 0.0003 cm⁻¹, ensuring a linear relationship between peak height or area and mole
188 fraction. The CRDS provides precise, highly sensitive measurements of gases in ambient air
189 with a temporal resolution of 5 seconds. The technique has been well validated for measuring
190 atmospheric CO, CO₂, and CH₄ mole fractions globally and at some Indian monitoring stations
191 (Chandra et al., 2016; Chen et al., 2013; Jain et al., 2021).

Deleted: analyzer

Deleted: fraction

Deleted: analyzer

Deleted: that

Deleted: techniques such as other

192 The standard cavity temperature of 45°C (throughout the measurement period) ensures
193 the necessary etalon mechanical stability of the measurement cavity. The sample air was taken
194 from the top of the building and above the tree canopy (5 meters above the instrument housing)
195 through a Teflon (PTFE) tube with an inner diameter of 3 mm using an external vacuum pump
196 with ~400 SCCM flow rate (residence time ~5.9 s). The air intake height is about 248 m.

Deleted: offers

Deleted: and

Deleted: the measurements of

Deleted: fraction,

Deleted: over

Deleted: In this study, the

Deleted: was maintained at

Deleted: to ensure

Formatted: Font colour: Black

Formatted: Font colour: Black

Formatted: Font colour: Black

Formatted: Font colour: Black

Deleted: 10

Deleted: and Teflon tube at

Deleted: .

Deleted: To better interpret the temporal variability in the atmospheric CO₂ mole fraction, we calculated the background CO₂ mole fraction at Sonipat. The background mole fraction are typically calculated from measurements over pristine sites free of local emission sources.

197 The Sonipat station, lying on the upwind side of Delhi, is a suburban station with
198 relatively cleaner air compared to the urban city centre. However, Sonipat cannot be considered
199 a pristine site due to the impact of local emissions from nearby industries and national
200 highways. We adopted (1) the fifth percentile of the daily data to characterise background mole
201 fraction at the site (Ammoura et al., 2014; Chandra et al., 2016; Jain et al., 2021), and (2) the
202 adaptive diurnal minimum variation selection (ADVS) method that considers the diurnal

Deleted: when

Deleted: Typically, two techniques are used to calculate background CO₂ mole fraction at such monitoring stations. The fifth percentile method is based on

Deleted: calculate the

Deleted: . The

233 minimum value as the daily background value (Apadula et al., 2019; Yuan et al., 2018). In this
234 study, the comparison between the fifth percentile and the ADVS methods showed similar CO₂
235 background values (see Fig. S1), and the ADVS method was used for further analysis. The
236 excess CO₂ mole fractions were then estimated by subtracting the hourly averaged values of
237 CO₂ from the background mole fraction.

238 The measurements of the atmospheric CH₄ mole fraction were also conducted with the
239 PICARRO G2301 GHG analyser. The GHG analyser employs the CRDS at 0.5 Hz to measure
240 CH₄ mole fraction. The mole fractions of CH₄ were determined using the ring-down time of
241 light intensity, similar to CO₂ mole fractions. Calibration was performed following the
242 guidelines of the National Oceanic and Atmospheric Administration Earth System Research
243 Laboratories (NOAA-ESRL, 2020) and the Integrated Carbon Observation System (ICOS)
244 protocol (Laurent, 2016), using NOAA standard calibration cylinders. Further details of the
245 calibration process are provided in Supplementary Section S1.

247 2.2.2 Trace gas measurements

248 In addition to the measurements of CO₂ and CH₄, we also utilised the measurements of trace
249 gases to establish the species interrelationships and to identify drivers of GHG sources. We
250 used a compact air-quality measurement instrument with gas sensors (CUPI-G) to continuously
251 measure air pollutants, including fine particulate matter (PM_{2.5}), nitric oxide (NO), nitrogen
252 dioxide (NO₂), and carbon monoxide (CO). The sensors used in CUPI-G are a palm-sized
253 optical PM_{2.5} sensor developed by Panasonic, the CO-B4 Carbon Monoxide Sensor, and the
254 NO-B4 Nitric Oxide Sensor, respectively. The sensitivity of the PM_{2.5} and CO sensors was
255 evaluated in Nagasaki, Japan (courtesy of Prof. Tomoki Nakayama), through intercomparisons
256 with reference-grade instruments employing a beta attenuation monitor (BAM) for PM_{2.5} and
257 non-dispersive infrared (NDIR) spectroscopy for CO measurements. The estimated unit-to-unit
258 variability was 29% for PM_{2.5} sensors and 21% for CO sensors. Further details on the sensor
259 specifications and the calibration methodology are described in Mangaraj et al. (2025).

261 2.2.3 Local meteorology measurements

262 A Vaisala Ceilometer lidar CL61 provides real-time measurements of cloud base height (CBH)
263 for up to five layers, along with depolarisation measurements, under all weather conditions. To
264 determine the Planetary boundary layer height (PBLH) from the range-corrected attenuated
265 backscatter data, the gradient method (Summa et al., 2013) and the Wavelet Covariance
266 Transform (WCT) method (Baars et al., 2008) were employed. Further details on PBLH

Deleted: S1). Therefore, we adopted one of

Deleted: methods (

Deleted:) here to report the background CO₂ mole fraction at Sonipat station.

Deleted: fraction

Deleted: fraction

Deleted: fraction

Deleted:

Deleted: collect continuous measurements of

Deleted: The CUPI-G was deployed on the roof of the I-Techpark building at IIT Delhi's Sonipat campus at the same location

Deleted: was installed on the rooftop of the I-Techpark building at IIT Delhi's Sonipat campus at the same location as the GHG analyser is located. The CL61 system is designed to provide...

282 calculations can be found in Rathore et al., (2025). An automatic weather station (AWS) by
283 Geonica, installed on the I-Tech building rooftop, collected meteorological data at 5-minute
284 intervals. The data, including ambient temperature, relative humidity (RH), atmospheric
285 pressure, wind speed and direction, precipitation, and incoming solar radiation, were retrieved
286 using Datagraph-W4K 2.1.3.0 software and exported in CSV format. All sensors were
287 meticulously calibrated and regularly cleaned to ensure accuracy and reliability.

Deleted: (

Deleted: was

289 2.3 Auxiliary data

290 2.3.1 ObsPack Data

291 To compare the seasonality of atmospheric CO₂ of Sonipat with other non-Indian sites in the
292 same latitudinal band, we used selected sites from the
293 obspack_co2_1_GLOBALVIEWplus_v10.1_2024-11-13 (Schuldt et al., 2024), The data was
294 averaged for five years from 2018 to 2022 for all stations except Boulder Atmospheric
295 Observatory, Colorado, (2011-2016), to compare the seasonality over different locations across
296 the globe.

Deleted: This dataset is constructed using the Observation Package (ObsPack) framework (Masarie et al., 2014). This product includes 625 atmospheric carbon dioxide datasets from observations made by 79 laboratories from 28 countries. The ObsPack dataset provides data for the period 1957-2023. We used the five-year averaged data for all sites except one (Boulder Atmospheric Observatory, Colorado) for 2018-2022 to further compare the seasonality over different locations across the globe.

Formatted: Font colour: Black

Formatted: Not Highlight

Formatted: Font colour: Black

298 2.3.2 Satellite CO₂ retrievals

299 Along with the ground-based in situ CO₂ measurements at the Sonipat monitoring station, we
300 also used column average dry air CO₂ mole fraction (XCO₂) retrievals from the Orbiting
301 Carbon Observatory-2 and 3 satellites (OCO-2 and OCO-3) (Crisp et al., 2017; Eldering et al.,
302 2017). We used the bias-corrected OCO-2 v11.1r data product for the period from February
303 2023 to December 2024. The OCO-3 satellite provides XCO₂ data at a repeat cycle of 16 days
304 with a spatial resolution of 1.60 km × 2.25 km (nadir observation), which increases the swath
305 area from ~3.0 km² to ~3.5 km². We used the bias-corrected OCO-3 v10.4r data product
306 (Eldering et al., 2019; Srivastava et al., 2020) for the period from February 2023 to December
307 2024.

Deleted:). The OCO-2 satellite provides data at a temporal frequency of 16 days with a spatial resolution of 1.29 km × 2.25 km (for nadir observations)

Deleted: temporal frequency

Deleted:)

309 2.3.3 FluxSat GPP

310 To study the Gross Primary Production (GPP) fluxes over Sonipat, we used FluxSat v2.2 native
311 GPP product computed at the spatio-temporal resolution of the MCD43C data set (daily at
312 0.05° spatial resolution (Schaaf et al., 2002; Wang et al., 2018). FluxSat v2.2 has been derived
313 from the MODerate resolution Imaging Spectroradiometer (MODIS) instruments on the NASA
314 Terra and Aqua satellites using the collection 6.1 MCD43C Bidirectional Reflectance
315 Distribution Function (BRDF)-Adjusted Reflectances (NBAR) (Joiner et al., 2018; Joiner and

332 Yoshida, 2020; Schaaf and Wang, 2021). FluxSat v2.2 is “calibrated” using a set of the
333 FLUXNET 2015 and OneFlux tier 1 (publicly released) eddy covariance (EC) data and has
334 been compared with independent data (i.e., not used in the calibration) as validation. We used
335 Global Gross Primary Production (GPP) estimates for 2023 in this study.

337 2.3.4 Ecosystem-proxy variables

338 We used two key ecosystem proxy variables to examine the carbon cycle dynamics at the
339 Sonipat station and in the IGP region. The Normalised Difference Vegetation Index (NDVI)
340 version 5 data from the Advanced Very High Resolution Radiometer (AVHRR) was used here
341 (Vermote and NOAA CDR Program, 2018). The NDVI CDR summarises surface vegetation
342 coverage activity based on measurements in the red and near-infrared spectral bands at daily
343 intervals and at a spatial resolution of $0.05^\circ \times 0.05^\circ$.

344 To understand the photosynthetic capacity of the regional ecosystem to assimilate
345 atmospheric CO₂, we used Solar-Induced Chlorophyll Fluorescence (SIF) retrievals from the
346 OCO-2 satellite (Frankenberg et al., 2014). The OCO-2 provides SIF data at a temporal
347 resolution of 16 days and a spatial resolution of 1.35 km × 2.25 km. The estimation of SIF
348 relies on evaluating the in-filling of solar Fraunhofer lines at 757 nm and 770.1 nm surrounding
349 the O₂ A-band (Frankenberg et al., 2014; Sun et al., 2018). We used bias-corrected SIF data
350 from OCO-2 v11r and v11.2r SIF data products.

352 2.4 Models

353 2.4.1 JAMSTEC's MIROC version 4 atmospheric chemistry-transport model (MIROC4- 354 ACTM)

355 We used the Model for Interdisciplinary Research on Climate version 4 (MIROC4),
356 atmospheric general circulation model (AGCM)-based chemistry-transport model (MIROC4-
357 ACTM; Patra et al., 2018), to simulate CO₂ mole fraction for this study. Simulations were
358 performed at a horizontal resolution of T42 spectral truncations (~2.8° latitude–longitude grid)
359 with 67 vertical hybrid-pressure layers between the Earth's surface and 0.0128 hPa (~80 km).
360 CO₂ tracers were simulated corresponding to fossil fuel combustion (FFCO₂), land biosphere
361 fluxes (LBCO₂), fire emissions (CO_{2fire}), and ocean exchanges (CO_{2ocn}) from different prior
362 (bottom-up) emissions sets (Chandra et al., 2022). FFCO₂ was simulated using the gridded
363 fossil fuel emission dataset (GridFED; Jones et al., 2021). LBCO₂ tracers were simulated using
364 two sets of terrestrial biosphere fluxes from the Carnegie-Ames-Stanford Approach (CASA)

- Deleted: -
- Deleted: study
- Deleted: of
- Deleted: -
- Deleted: (Vermote and NOAA CDR Program, 2018). This dataset consists of daily NDVI values retrieved from the National Oceanic and Atmospheric Administration's (NOAA) Climate Data Record (CDR) of AVHRR Surface Reflectance.
- Deleted: the
- Formatted: Not Highlight
- Deleted: . The NDVI CDR provides
- Formatted: Not Highlight
- Deleted: output on
- Deleted: global grid with a
- Deleted: degrees latitude by
- Deleted: degrees longitude from 1981 to the present.
- Deleted: the
- Deleted:
- Deleted: chlorophyll
- Formatted: Not Highlight
- Deleted: for February 2023 to December 2024.
- Formatted: Indent: First line: 1.27 cm
- Deleted: ;Watanabe et al., 2008
- Deleted: an
- Deleted: of long-lived gases (CO₂, CH₄, N₂O, SF₆)
- Deleted:) (Bisht et al., 2021; Chandra et al., 2021; Patra et al., 2017, 2018). CO₂ tracers were simulated corresponding to the
- Deleted: sets of prior (bottom-up) emissions (Chandra et al., 2022).

391 biogeochemical model (Randerson et al., 1997) and Vegetation Integrative Simulator for Trace
392 Gases (VISIT) (Ito, 2019).

Deleted: For this study, we use simulated total CO₂ mole fraction and tracers.

394 2.4.2 CarbonTracker (CT) inverse model

395 To understand the temporal pattern of atmospheric CO₂ mole fraction over the study station
396 and the IGP region, we used simulated CO₂ mole fraction from an inverse modelling
397 framework CarbonTracker (CT) (Peters et al., 2005). Here, we used the CarbonTracker 2022
398 release (CT2022), which incorporated two-way nesting of the offline atmospheric tracer
399 transport model TM5, supporting coarse-resolution global data and high-resolution regional
400 data (Krol et al., 2004). The TM5 model in CT2022 was driven with meteorology from the
401 ERA-interim reanalysis provided by the European Center for Medium-Range Weather
402 Forecasts (ECMWF). The CT2022 inverse model simulated atmospheric CO₂ mole fraction by
403 correcting the prior specifications of CO₂ sources and sinks in the model by assimilating global
404 in situ observations. In this study, we used the CT2022-simulated CO₂ mole fraction from
405 February 2023 to October 2023.

Deleted:)

Deleted: globally

Deleted: regionally

Deleted: ECMRWF) {Citation}.

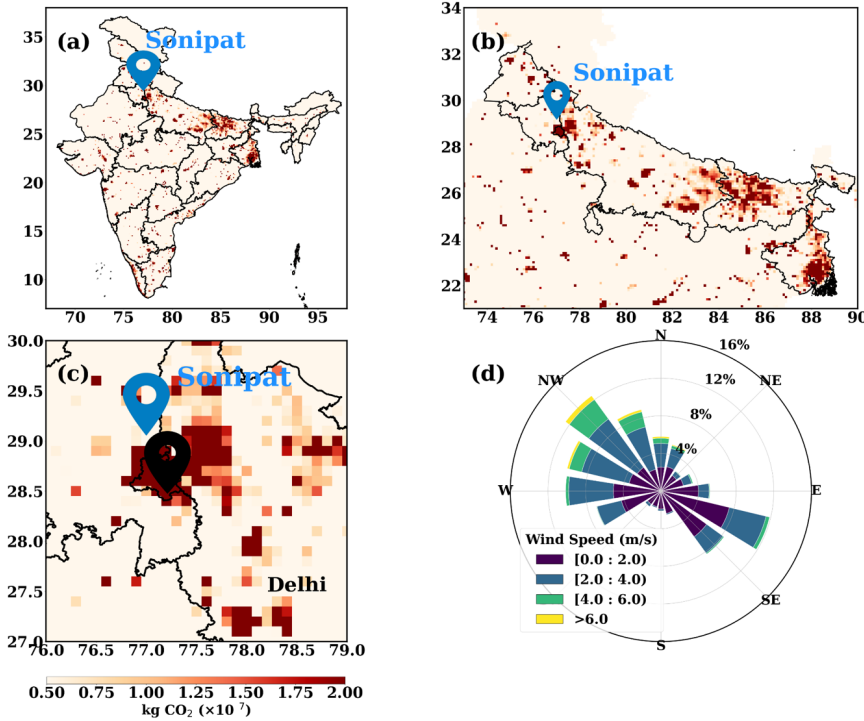
407 2.4.3 GEOS-Chem inverse model

408 To study the seasonality of the fluxes over Sonipat, we used a four-dimensional variational
409 (4D-Var) assimilation system with the GEOS-Chem global chemical transport model
410 (CTM; Philip et al., 2019, 2022). The GEOS-Chem 4D-Var system was constrained with XCO₂
411 retrievals from the OCO-2 satellite (Philip et al., 2022), following the protocol of the OCO-2
412 v10 Multi-model Intercomparison Project (MIP) (Byrne et al., 2017; Liu et al., 2014). The Net
413 Ecosystem Exchange (NEE) fluxes for 2023 at a spatial resolution of 1° × 1°, constrained with
414 the OCO-2 Land Nadir and Land Glint observational modes are used here.

416 2.4.4 Mi CASA terrestrial biospheric model

417 We also used simulated CO₂ fluxes from a terrestrial biospheric model (TBM) in this study.
418 The Más informada Carnegie-Ames-Stanford-Approach (Mi CASA) model (Weir, 2024), a
419 comprehensive update to the CASA – Global Fire Emissions Database, version 3 (CASA-
420 GFED3) product, was utilised here (Chen et al., 2023; Potter et al., 1993). Mi CASA provides
421 daily global data at 0.1° resolution from January 2001 to December 2023. This includes carbon
422 flux variables from sources such as net primary production (NPP), heterotrophic respiration
423 (Rh), wildfire emissions (FIRE), and fuel wood burning emissions (FUEL). The model is

430 driven with meteorological data from NASA's Modern-Era Retrospective analysis for Research
 431 and Application, Version 2 (MERRA-2).



432
 433 **Figure 1:** Anthropogenic CO₂ emissions over (a) India (b) IGP and (c) Sonipat/Delhi derived
 434 from the EDGAR emission inventory for 2021. (d) Annually averaged wind patterns over
 435 Sonipat for February 2023 – January 2024.

436
 437
 438 **3. Results and discussions**

439 **3.1 CO₂ measurements at Sonipat station**

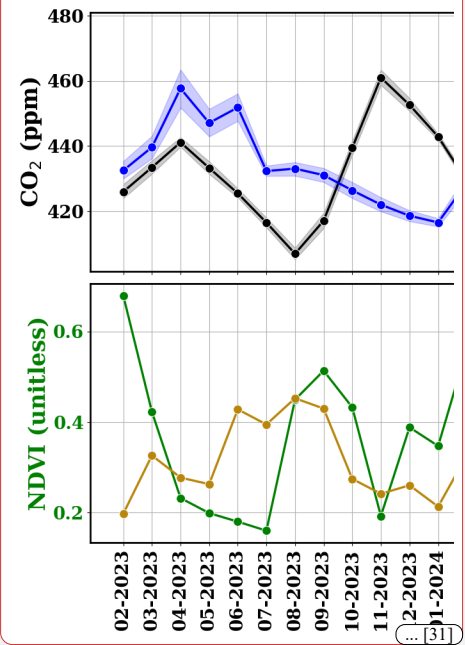
440 Figures 1(a-c) illustrate the annual mean anthropogenic CO₂ emissions over India, IGP and
 441 Delhi/Sonipat for 2021 based on the EDGAR emission inventory, a major hotspot of
 442 anthropogenic CO₂ emissions. The dominant wind direction over Sonipat was from the
 443 northwest during the study period, highlighting influence from upwind sources of pollution and

~~Deleted:~~ Previous studies used the MERRA-driven CASA GFED to investigate the carbon cycle dynamics (Campbell et al., 2008; Hammerling et al., 2012; Kawa et al., 2010; Ott et al., 2015; Weir et al., 2021a, b). We used Mi CASA model simulated NEE, NPP, and Rh fluxes over the Sonipat station for this study.

~~Formatted:~~ Strikethrough

~~Deleted:~~ ¶ ... [30]

~~Deleted:~~ Figure 1(a) shows hourly averaged time series of atmospheric CO₂ mole fraction at the Sonipat station from February 2023 to January 2025. During this period, hourly CO₂ varies in the range from ~380 ppm to ~550 ppm, with the highest values observed in November 2024 indicating the large variability in the regional CO₂ build-up at the study location. The strong seasonal and diurnal variations are evident during the entire study period. In general, minimum variability and lowest mole fraction of CO₂ are found from July to August, while strong variability and high mole fraction are visible from October to November. We found annual mean CO₂ mole fraction of 440.8 ± 19.7 ppm during the study period. Table S1 compares the annual mean CO₂ mole fraction values with other measurement network stations in India. Interestingly, the annual mean values for different stations in India, even rural sites like Gadanki and urban sites like Ahmedabad, have consistent values. ¶



~~Deleted:~~ b) and l(

~~Deleted:~~ and it is observed that the Delhi NCR is a

~~Deleted:~~ Figure 1(d) shows that the

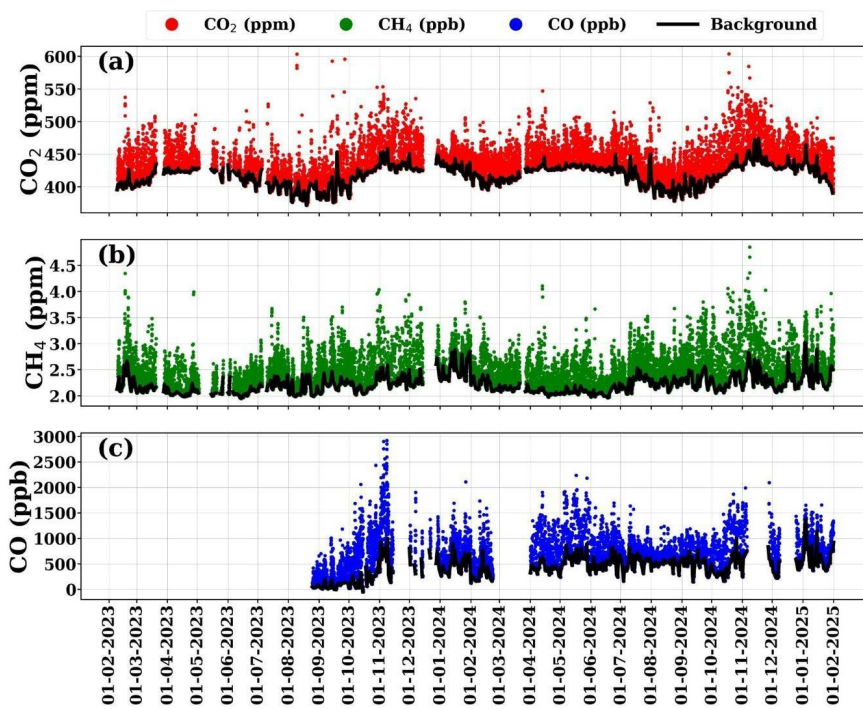
~~Deleted:~~ during the study period

~~Formatted:~~ Subscript

~~Deleted:~~ , indicating significant

505 greenhouse gases (Figure 1d). Seasonal changes in meteorological parameters (air temperature,
 506 relative humidity, rainfall and wind; Figures S2 and S3) were also analysed alongside CO₂ to
 507 better understand the role of meteorology in Sonipat. In this study, we focus on seasonal and
 508 diurnal CO₂ variability and compare these patterns with those at other stations in India and in
 509 the same latitudinal band across the globe to uncover the unique aspects of CO₂ dynamics over
 510 Sonipat and the IGP.

Deleted: . To better understand the local meteorology, we analysed the seasonal variations of various
 Deleted: such as
 Deleted: wind speed, wind direction and
 Deleted: (Fig.
 Deleted:). Figure
 Deleted: presents the seasonally averaged wind rose diagrams over Sonipat. It is evident that the predominant wind pattern is from the northwest.
 Deleted: as well.



511
 512 **Figure 2:** (a) Hourly averaged time series of atmospheric (a) CO₂, (b) CH₄, and (c) CO mole
 513 fraction for the study period (February 2023 to January 2025) over Sonipat. The thick black
 514 line represents the background mole fraction estimated using the ADVS method.

516 Figure 2 presents the hourly averaged time series of atmospheric (a) CO₂, (b) CH₄, and
 517 (c) CO mole fractions at Sonipat during the study period (February 2023 to January 2025).
 518 Hourly CO₂ mole fractions range from ~380 ppm to ~550 ppm, indicating strong monthly
 519 variations in CO₂ mole fractions at the monitoring station. The lowest CO₂ mole fractions were
 520 observed from July to August, which coincided with weak CO and strong CH₄ values. The

Formatted: Space Before: 6 pt

531 highest mole fractions of CO₂ were observed from October to November, coinciding with the
532 highest mole fractions of CO and CH₄. We found an annual mean CO₂ mole fraction of
533 440.8±19.7 ppm for 2024 and compared it with those from other monitoring stations across
534 India (Table S1). Interestingly, despite differences in site characteristics, the annual mean CO₂
535 levels at rural stations like Gadanki and urban stations like Ahmedabad are comparable,
536 whereas Sonipat shows distinctly higher values.

Formatted: Font colour: Black

537 3.2 Seasonal variability

538 3.2.1 Seasonality of in situ observations

539 Figure 3 shows the monthly mean atmospheric CO₂ mole fractions during the study period. A
540 shaded background has been used to distinguish the seasonal regimes used in this study. The
541 monthly mean CO₂ mole fraction shows a maximum in November (post-monsoon season) and
542 a minimum in August (monsoon season) in both years. The observed seasonal mean of CO₂
543 during different seasons were 440.8±19.7 ppm (pre-monsoon), 422.6±23.3 ppm (monsoon),
544 456.4±30.8 ppm (post-monsoon), and 440.5±19.7 ppm (winter).

Deleted: 2

Deleted: fraction

Deleted: The

Deleted: region represents a 95 percent confidence interval of

Deleted: . The monthly mean mole fraction of CO₂

Deleted: during

Deleted: The average seasonal mean values of CO₂

Deleted: are

Deleted: ±

Deleted: ±

Deleted: ±

Deleted: ±

Deleted: cycle of

Deleted: is mostly

Deleted: One of the key factors that controls the local variability of atmospheric CO₂ is

Deleted:). This

Deleted: Strong vertical mixing in a well-developed boundary layer can dilute GHG mole fraction near the surface. Therefore, the seasonal changes in the PBLH affect the atmospheric CO₂ mole fraction near the surface. Figure 2(a) shows that the minimum values in PBLH during pre-monsoon months and maximum values during winter.

Deleted: fraction as compared

Deleted: the winter months

Deleted:

545 The seasonal change in CO₂ mole fractions over the monitoring station is governed by
546 the strength of emission sources, photosynthetic activity (biospheric fluxes), local meteorology
547 and atmospheric transport. The planetary boundary layer height (PBLH), which is determined
548 by local meteorology, strongly influences CO₂ mole fractions. PBL is the lowest layer within
549 the troposphere, where temperature and wind speed variations are integral in modulating its
550 height. During pre-monsoon, deep convection due to the well-developed PBLH from the
551 surface to the upper troposphere results in lower mole fractions of CO₂, while the weakly
552 developed PBLH in winter leads to higher CO₂ (Baker et al., 2012; Kar et al., 2004; Park et al.,
553 2009; Patra et al., 2011; Randel and Park, 2006).

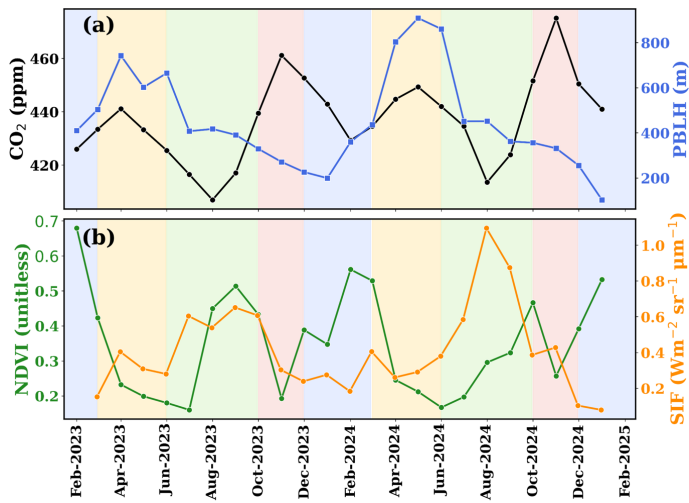


Figure 3: (a) Monthly variations of atmospheric CO₂ mole fraction (black) and PBLH (blue) and (b) NDVI (green) and SIF (orange) over the Sonipat monitoring station during the study period. The shaded background represents different seasons: yellow (pre-monsoon), green (monsoon), red (post-monsoon) and blue (winter).

The seasonal change in CO₂ was examined using two different vegetation indices (normalised difference vegetation index, NDVI, and solar-induced fluorescence, SIF) to assess the role of the biosphere in CO₂ mole fractions over Sonipat. Both NDVI and SIF have been widely used as indicators of vegetation cover and photosynthetic activity (Aburas et al., 2015; Nath, 2014). Our analysis shows a strong inverse relationship between CO₂ levels and NDVI, as illustrated in Figure 3b. A noticeable decrease in atmospheric CO₂ mole fraction is observed at the onset of the monsoon (June), with increased vegetative activity continuing until September. Increased vegetation cover increases photosynthetic carbon uptake by the biosphere. However, as vegetation activity decreases from the post-monsoon to winter and pre-monsoon seasons, photosynthetic carbon uptake decreases, leading to a rise in atmospheric CO₂. Spearman's rank correlation analysis showed a weak and statistically insignificant relationship between CO₂ and NDVI ($\rho = -0.09$, $p = 0.74$). In contrast, CO₂ exhibited a moderate negative correlation with SIF ($\rho = -0.42$, $p = 0.07$). The negative correlation with SIF is consistent with enhanced biospheric uptake during periods of increased photosynthetic activity. Similar studies (Metya et al., 2021; Sreenivas et al., 2016; Tiwari et al., 2014), over India exhibited a strong dependence of CO₂ seasonality on local vegetative carbon uptake.

Deleted: To better understand the

Deleted: patterns of

Deleted: mole fraction, we

Deleted: its relationship with the

Deleted: (

Deleted:)

Deleted: (SIF).

Deleted: are

Formatted: Not Superscript/ Subscript

Deleted: Fig. 2.

Deleted: 2(b) reveals that vegetation growth starts with the onset of the monsoon season. An enhanced vegetation cover over the region from August and a

Deleted: evident.

Deleted: shows an increase in the

Deleted: , which decreases atmospheric CO₂ mole fraction.

Deleted: declines

Deleted: The negative correlation of NDVI versus CO₂ mole fraction was found for most locations in India

Deleted: indicating the

Deleted: the

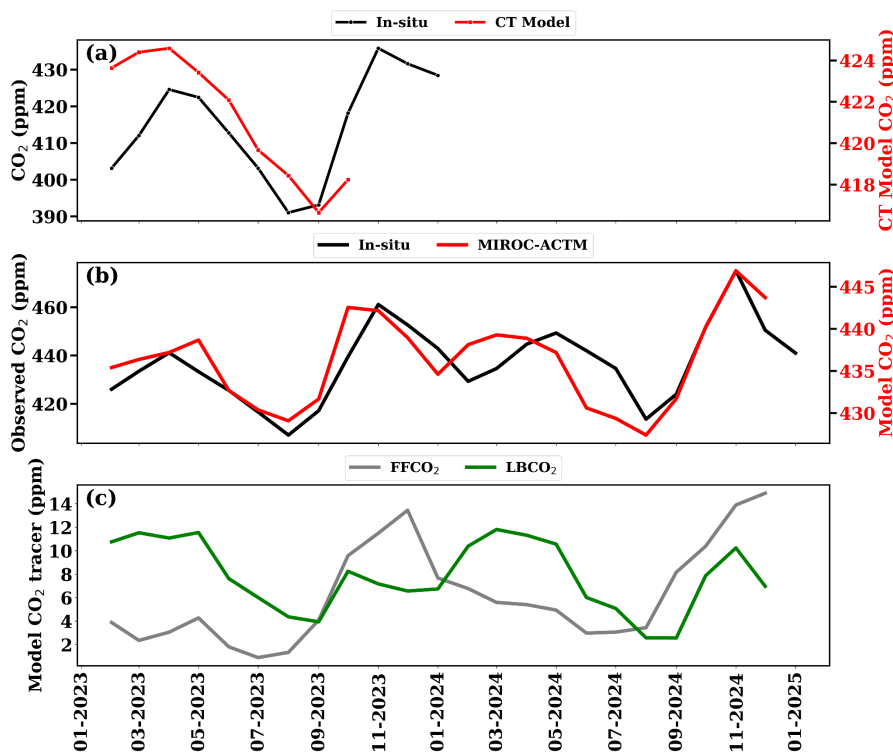
Deleted:

622 A sharp decrease in the seasonal mean (~18 ppm) ~~was noted~~ from pre-monsoon to
 623 monsoon, attributed to enhanced photosynthetic activity around the measurement site, driven
 624 by abundant soil moisture. A further decrease in CO₂ mole fraction is also observed as the
 625 monsoon progresses, with minimum CO₂ mole ~~fractions~~ observed in August. The decreases in
 626 temperature (due to cloudy, overcast conditions prevailing during these months) reduce leaf
 627 and soil respiration, thereby enhancing carbon uptake (Jing et al., 2010; Patil et al., 2014).
 628 Further, an increase in CO₂ mole fraction (~34 ppm) is observed during post-monsoon,
 629 ~~reflecting~~ higher ecosystem ~~respiration~~ (Sharma et al., 2014) and ~~enhanced soil microbial~~
 630 ~~activity~~ (Fan & Forkel, 2025; Munksgaard et al., 2022), ~~particularly from nocturnal respiration~~
 631 ~~prior to crop harvest~~. The gradual decline in NDVI during this period indicates reduced CO₂
 632 uptake by vegetation. This season ~~coincided~~ with crop-burning episodes in northern India,
 633 ~~which~~ significantly increased CO₂ mole ~~fractions~~. A sharp decrease (~16 ppm) in the seasonal
 634 mean during winter is evident compared to the post-monsoon. The shallow PBLH and winds
 635 from western IGP that transport crop-burning residue contribute to the enhanced mole fraction
 636 during winter. Table S2 compares the seasonal amplitude and the peak and drawdown months
 637 at the measurement site with those in similar studies ~~across~~ India. Sonipat exhibits higher
 638 seasonal amplitudes than other sites. However, a similar pattern in CO₂ peak and drawdown
 639 months is evident in other monitoring stations.

640 3.2.2 ~~Seasonal constraints~~ from model and satellites

641 Figure 4(a) shows the comparison of ground-based mole fraction of CO₂ with CarbonTracker
 642 inverse model (CT2022) simulated mole fraction (see different y-axis). The model outputs
 643 beyond October 2023 were not publicly available. In general, the CT2022 model-simulated
 644 mole ~~fractions~~ are much lower than ~~the~~ observed mole ~~fractions~~ at the Sonipat station. The
 645 discrepancy ~~is~~ mainly due to the ~~model's~~ coarser resolution. Nevertheless, the ~~model-simulated~~
 646 seasonal pattern of CO₂ mole fraction ~~is broadly~~ in agreement with observations (Figure 4).
 647 The CT2022 model simulates a minimum mole fraction of 416 ppm ~~in~~ September, whereas in
 648 situ measurements show a minimum of 407 ppm ~~in~~ August. The CT2022 model exhibits higher
 649 mole ~~fractions~~ during the pre-monsoon season, ~~consistent with~~ in situ data. Note that most
 650 global and regional chemical transport models were unable to reproduce the large seasonal
 651 ~~amplitude~~ of surface-based measured atmospheric CO₂ mole ~~fractions~~ at any of the monitoring
 652 stations in India with different ~~ecosystems~~ (Lin et al., 2018; Philip et al., 2022).

- Deleted: is visible
- Deleted: . This is
- Deleted: a
- Deleted: fraction
- Formatted: Font colour: Black
- Deleted:
- Formatted: Font colour: Black
- Formatted: Font colour: Black
- Deleted: which is associated with
- Deleted: productivity
- Deleted: an enhancement in soil microbial activity (Kirschke et al., 2013).
- Formatted: Font colour: Black
- Formatted: Font colour: Black
- Formatted: Font colour: Black
- Formatted: Font colour: Black
- Deleted: coincides
- Deleted: . Crop residue burning activities
- Deleted: contribute to
- Deleted: fraction
- Deleted: over
- Deleted: Constraints
- Deleted: 3
- Deleted: the
- Deleted: fraction
- Deleted: fraction
- Deleted: could be
- Deleted: representativeness issue, due to the
- Deleted: model spatial
- Deleted: simulated with the model is
- Deleted: broad
- Deleted: Fig. 3
- Deleted: the seasonal variability with
- Deleted: during
- Deleted: mole fraction
- Deleted: during
- Deleted: fraction
- Deleted: similar to
- Deleted: magnitude
- Deleted: fraction for
- Deleted: land



687 **Figure 4:** (a) Monthly mean background CO₂ mole fraction over Sonipat (estimated using the
 688 ADVS method) compared to CarbonTracker (CT2022) model-simulated values at daytime
 689 (13:00 – 16:00). Note that the left y-axis represents surface mole fraction from in situ
 690 measurements, and the right y-axis represents CT2022-simulated mole fraction. (b) comparison
 691 of simulated mole fraction of atmospheric CO₂ from MIROC-ACTM with in situ
 692 measurements at Sonipat and (c) monthly averaged time series of different tracers from the
 693 MIROC-ACTM.
 694
 695

696 Figure 4(b) shows the comparison of atmospheric CO₂ mole fractions over Sonipat with
 697 the simulated mole fraction of CO₂ from the MIROC4-ACTM model. Similar to CT2022,
 698 MIROC captures the seasonal pattern of CO₂, but fails to capture the actual seasonal amplitude
 699 over Sonipat. Figure 4(c) presents the monthly averaged time series of model-simulated CO₂
 700 tracers. The fossil fuel tracer (FFCO₂) exhibits a peak in the post-monsoon period, followed by
 701 a gradual decrease through the end of winter. The shallow PBLH during this time traps
 702 vehicular emissions from NH-44 and industrial sources upwind of the monitoring station.

Deleted: [32]

Deleted: 3:
 Formatted: Font: Not Bold

Deleted:

Deleted:

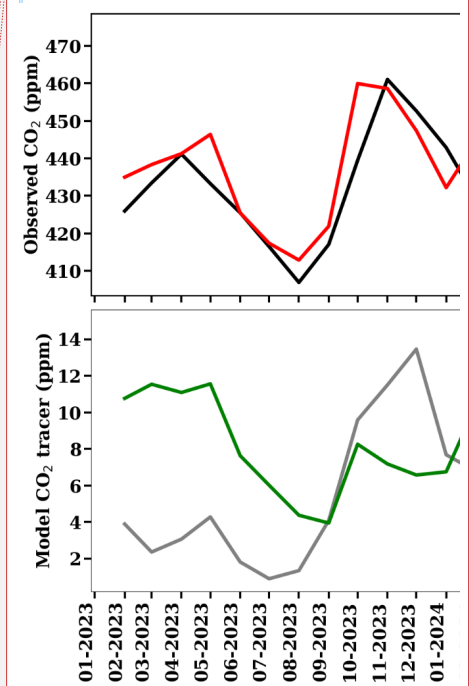


Figure 4: (a) Comparison...

Deleted: b

Deleted: a) presents

Deleted: fraction of CO₂

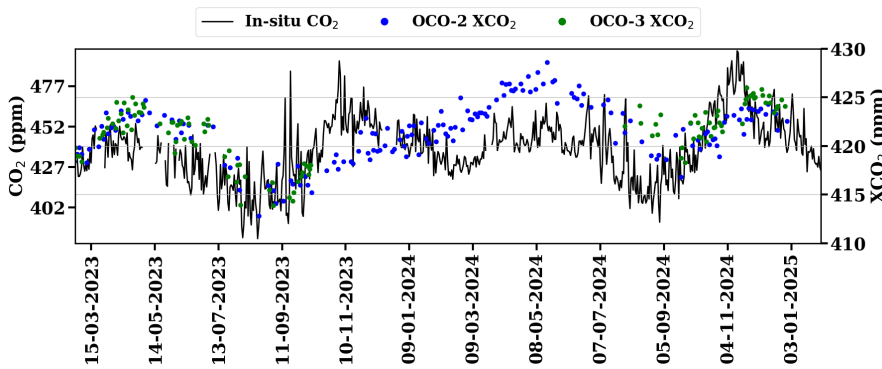
Deleted: The model has well captured

Deleted: it

Deleted: The highs during post-monsoon and the drawdown during pre-monsoon show a strong correlation with in situ measurements. Figure 4(b)

Deleted: post-monsoon with a gradual decrease in winter

721 resulting in higher FFCO₂. With the development of the PBLH in the pre-monsoon, FFCO₂
 722 shows a gradual decrease, and rainfall during the monsoon results in minimum values during
 723 this time. The biospheric tracer (LBCO₂) shows a peak during the pre-monsoon, driven by dry
 724 soil conditions and a lack of vegetation and a drawdown during the monsoon. A sharp increase
 725 in LBCO₂ is observed during the post-monsoon season, coinciding with the harvest period at
 726 the monitoring station. Being surrounded by agricultural land, Sonipat is prone to emissions
 727 from crop residue burning around and upwind of the monitoring station. Both models
 728 underestimate these enhancements from regional sources.



729
 730 **Figure 5:** Daily variations of atmospheric CO₂ mole fraction from in situ measurements over
 731 Sonipat (left y-axis) with column average CO₂ mole fraction (XCO₂) from the OCO-2 (ppm)
 732 and OCO-3 (ppm) satellite instruments (right y-axis).

733
 734 Figure 5 compares XCO₂ from OCO-2 and OCO-3 satellites with ground-based CO₂
 735 measurements at Sonipat during the study period. XCO₂ reveals a similar seasonal pattern with
 736 high mole fraction during the pre-monsoon season, followed by a drawdown in CO₂ mole
 737 fraction during the monsoon season and a further gradual increase in CO₂ during the post-
 738 monsoon and winter. Although the satellite column data captures the monthly variability
 739 reasonably well, it fails to capture the sharp increase in mole fraction during the post-monsoon.
 740 This post-monsoon enhancement from crop residue burning at the monitoring station, along
 741 with additional transport from Punjab, highlights the limitations of high-resolution satellite data
 742 in capturing regional scale enhancements.

Deleted: a drawdown
Deleted: monsoon, which coincides with observed CO₂ mole fraction. The post-monsoon peak can be attributed to the added emissions from crop residue burning, which is a characteristic of the site. The drawdown in monsoon can be attributed to the added soil moisture and increased CO₂ uptake by plants during this time (further discussed in section 3.4).

Deleted: presents
Deleted: and a drawdown in monsoon. The peak can be attributed to

Deleted: this time

Deleted: similar enhancement of

Deleted: visible

Deleted: which coincides

Deleted: over the site. The lack

Moved down [1]: Figure 5 compares XCO₂ from OCO-2 and OCO-3 satellites with ground-based CO₂ measurements at Sonipat during the study period.

Moved down [2]: Although the satellite column data captures the monthly variability reasonably well, it fails to capture the sharp increase in mole fraction during the post-monsoon.

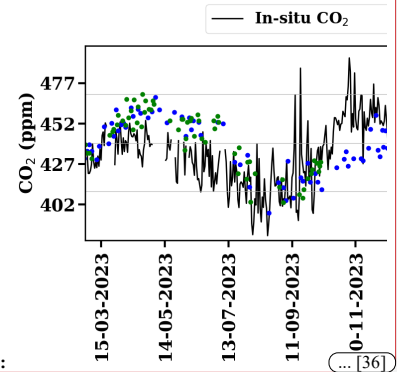
Deleted: vegetation with added CO₂ from crop residue burning contributes to this enhancement. The drawdown in mole fraction during the monsoon season is due to we... [33]

Deleted: The XCO₂ reveals a similar seasonal pattern with high mole fraction during the pre-monsoon season, fo... [34]

Deleted: This enhancement during the post-monsoon season can be attributed to crop residue burning over the mor... [35]

Deleted: local

Deleted:



Deleted: ... [36]

Formatted: Font: Not Bold

Moved (insertion) [1]

Deleted: 3.2.3 Comparison with data from other monitoring stations... [37]

Moved (insertion) [2]

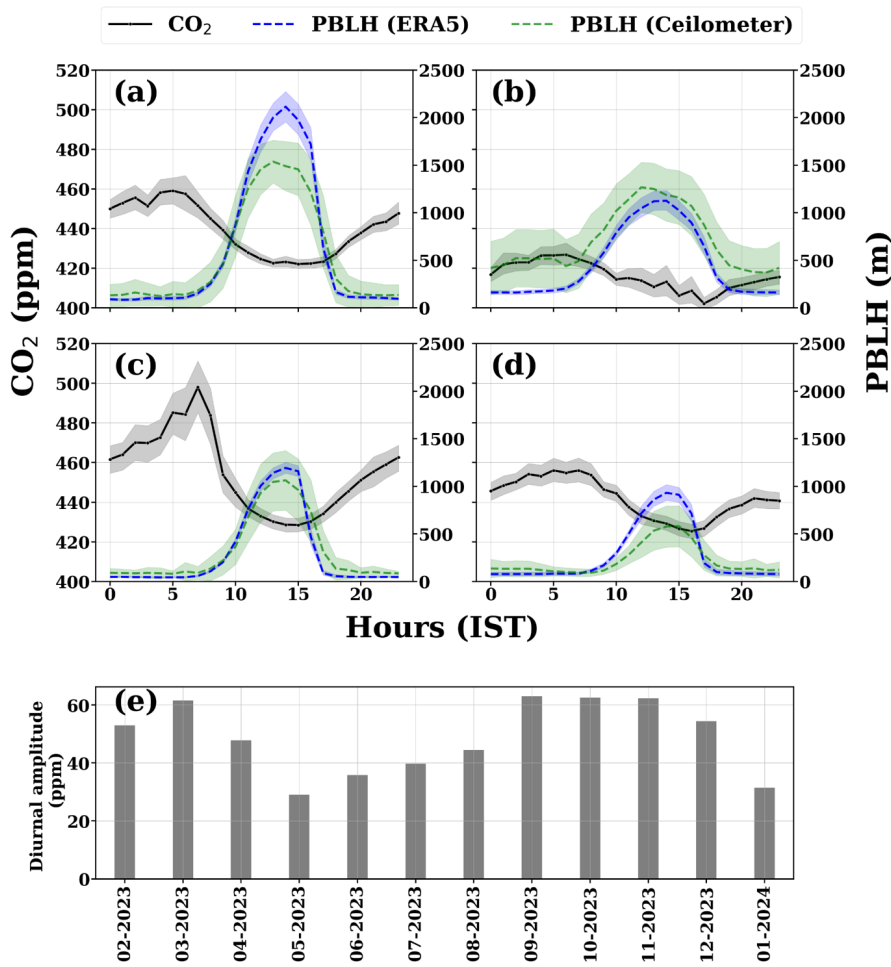


Figure 6: (a-d) Seasonally-averaged diurnal variation of atmospheric CO₂ over the Sonipat station during the pre-monsoon (MAM), monsoon (JJAS), post-monsoon (ON) and winter (DJF) seasons with planetary boundary layer heights (blue denotes PBLH from ERA5 and green denotes PBLH derived from Ceilometer), (e) monthly variation of the diurnal amplitude of CO₂ from February 2023 to January 2024.

3.3 Diurnal variability

Figure 6 (a-d) presents the averaged diurnal variation of atmospheric CO₂ mole fractions along with PBLH from ERA5 and Ceilometer at Sonipat during four seasons for the

Moved down [3]: (a) Comparison of the seasonal variability of atmospheric CO₂ over Sonipat monitoring station with various locations in the same latitudinal band. (b) Comparison of the seasonal amplitude between Indian (coloured bars) and international monitoring stations (grey bars). Indian stations include Shadnagar (SDN), Sinhadgad (SNG), Ahmedabad (AHM), Mohali (MHL), Gadanki (GDN), and Sonipat (SNT). International stations include Mauna Loa (MLO), South Carolina (SCT), Shenandoah National Park (SNP), Walnut Grove, (WGC), Moody (WKT) and Boulder (BAO). For all international stations except BAO, the five-year average (2018 - 2022) has been chosen for the seasonality. For BAO, 2011 - 2016 has been used.

Moved down [4]: The monthly average of the entire study period (February 2023 - January 2025) has been used for this comparison.

Moved down [5]: The diurnal amplitude shows large month-to-month variation with an increasing trend from May to September 2023 and a decreasing trend till February 2024.

Deleted: Sonipat exhibits very high seasonal amplitude (~ 60 ppm) compared to other sites (~ 15 ppm) across the globe, however, the seasonal amplitude is around 35 ppm at Ahmedabad. The major attribution to the high seasonal amplitude of CO₂ at Sonipat occurs during post-monsoon (Fig. 6a). This high amplitude for November has been observed during 2023 and 2024 (see Fig. 2), a characteristic of the Sonipat station. The high seasonal amplitude is associated with the crop residue burning season over Haryana and Punjab (further discussed in section 3.5). Being surrounded by agricultural land, Sonipat is prone to emissions from crop residue burning. The location of the measurement site in IGP on the downwind of Punjab is a major reason for this strong seasonal variability compared to other sites in the same latitudinal band.

3.3 Diurnal variability

Figure 7 (a-d) presents the averaged diurnal variation of atmospheric CO₂ mole fraction and PBLH at Sonipat during four seasons for the first year of the study (2023). The diurnal variability has been examined separately for the two years to exclude the influence of growth rate on the diurnal amplitude. Figure S4 presents the diurnal variation for the second year of the study. All the seasons exhibit a similar diurnal pattern with maximum mole fraction in the early morning hours (05:00 - 08:00 am) and minimum mole fraction during the late afternoon hours (2:00 - 3:00 pm). Figure 7(e) shows...

Deleted: The lowest diurnal amplitude of about 29 ppm is observed in May, while the highest amplitude at about 63 ppm is observed in September/October (Figure 7(e)). We found that the post-monsoon season exhibited the highest diurnal variability (~ 60 ppm), followed by the pre-monsoon season (~ 35 ppm), winter season (~ 30 ppm) and the monsoon season (20 ppm). The same was observed for...

Formatted: Font: Bold

Formatted: Indent: First line: 0 cm, Space After: 0 pt

Deleted: The seasonal differences observed in the CO₂ diurnal amplitudes can be attributed to changes in local meteorology and biospheric activity over the monitoring station. A key factor that drives the diurnal variability of CO₂ is the PBLH, which depends on local meteorology. The observed diurnal cycle of CO₂ is closely associated with the diurnal variation of the PBLH (Fig. 7). Figure S5 pres...

959 first year of the study (February 2023 – January 2024). Figure S4 presents the diurnal variation
960 for the second year of the study. The diurnal cycle has been analysed separately for each year,
961 combining available PBLH data. All seasons exhibit a similar diurnal pattern, with maximum
962 CO₂ mole fractions in the early morning hours (05:00 - 08:00 am) and minimum mole fractions
963 in the late afternoon hours (2:00 - 3:00 pm). The observed diurnal cycle of CO₂ is closely
964 associated with the development of PBLH during the day (Figure 6). The peak in CO₂ mole
965 fraction during the morning hours can be attributed to the fumigation effect, and a well-mixed
966 PBL dilutes CO₂ mole fractions during the afternoon hours.

967 Photosynthetic activity is another key driver of diurnal variability at Sonipat, a
968 characteristic observed in rural areas with vegetative cover (Imasu & Tanabe, 2018). Strong
969 vegetative uptake of CO₂ during the monsoon results in minimum daytime CO₂ mole fractions,
970 and the lack of vegetation during post-monsoon contributes to maximum daytime CO₂ mole
971 fractions during this season. The diurnal variation of GHGs reported by several studies
972 (Nishanth et al., 2014; Patil et al., 2014; Sharma et al., 2014) from different parts of the country
973 shows a similar trend. The same was observed for 2024 as well (Figure S4). The diurnal
974 variability of CO₂ over Sonipat is driven by biospheric activity and local meteorology.

975 Figure 6(e) shows the monthly average variation in diurnal amplitude (difference between the
976 maximum and minimum mole fraction of CO₂ in the diurnal cycle) during the first year. The
977 lowest diurnal amplitude of about 29 ppm is observed in May, while the highest amplitude at
978 about 63 ppm is observed in September/October. We found that the post-monsoon season
979 exhibited the highest diurnal variability (~60 ppm), followed by the pre-monsoon (~35 ppm),
980 winter (~30 ppm), and monsoon (~20 ppm) seasons.

982 3.4 Drivers of CO₂ seasonality

983 The contribution of biospheric fluxes in driving the CO₂ mole fraction over Sonipat (for
984 2023) was analysed in Figure 7. Figure 7(a) shows the simulated data from the Mi CASA
985 biosphere model along with the monthly averaged mole fractions of CO₂ and daytime CO₂
986 (06:00 – 18:00). Figure 7(b) presents the simulated NEE from GEOS-Chem and GPP from
987 FluxSat, along with the monthly averaged mole fractions of daily-mean and nighttime CO₂
988 (18:00 – 06:00). Positive NEE values indicate a net exchange of CO₂ from the biosphere to the
989 atmosphere. On the other hand, a negative NEE value (when NPP exceeds Rh) suggests the
990 uptake of CO₂ from the atmosphere to the biosphere.

Deleted: CO₂

Deleted: is the photosynthetic activity of the surrounding vegetation

Deleted: The combined effect of photosynthetic activity and a well-mixed PBLH (~1.3 km) during the afternoon hours in the post-monsoon season results in high diurnal variability. The low mole fraction during afternoon hours in the pre-monsoon season can be attributed to the dense PBLH (~2 km). The low diurnal variability during winter is due to the shallow PBLH (~900 m) and local meteorological conditions like weak winds. The delay in the evolution of the boundary layer could potentially result in a delayed, more pronounced fumigation peak during the winter season. Vegetative uptake of CO₂ is maximum during the monsoon season, and the poorly mixed PBL (~1.1 km) due to cloudy conditions contributes to minimum mole fraction and variability of CO₂ during this season.

Deleted: variability

Deleted: Fig. 8.

Deleted: 8

Deleted: fraction

Moved down [6]: NPP is the net amount of CO₂ retained in the biosphere. Rh is the amount of CO₂ emitted into the atmosphere due to the decomposition of organic matter by microorganisms in the soil.

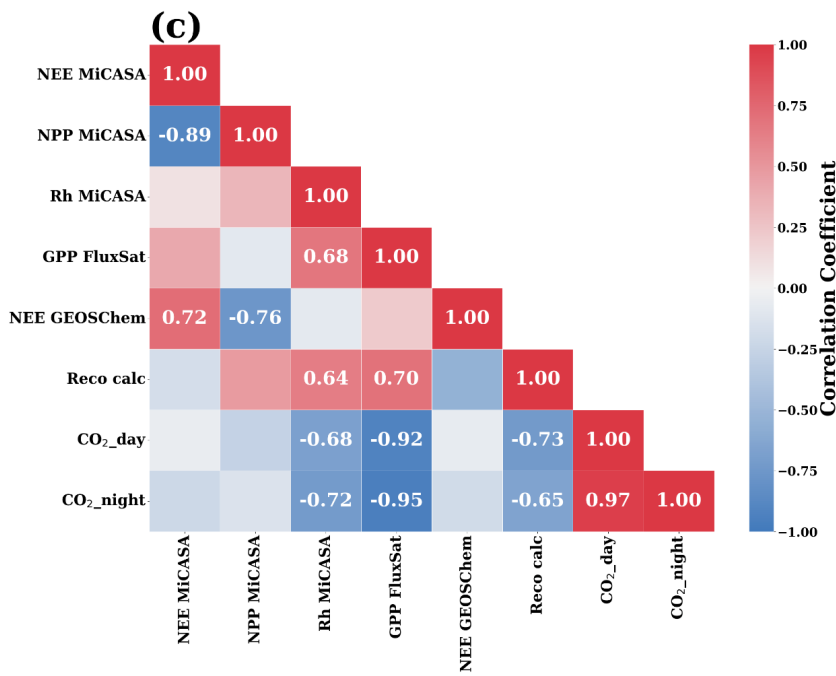
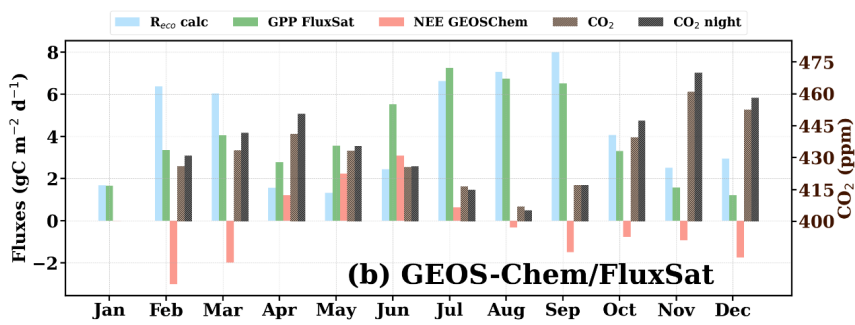
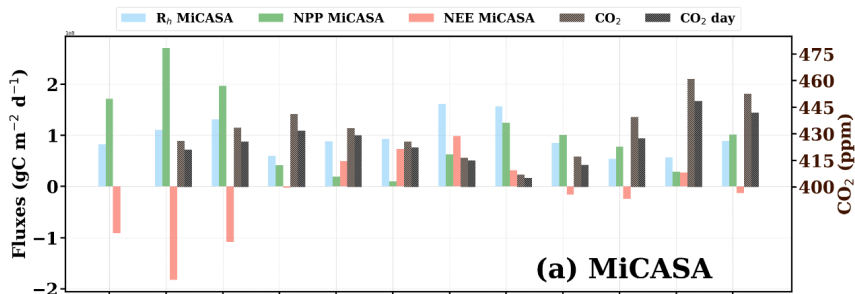
Deleted: The NEE flux represents the net carbon exchange between terrestrial ecosystems (difference between Rh and NPP).

Deleted: Figure 8

Deleted: fraction

Deleted: The GPP fluxes, a measure of carbon uptake by plants is also very high during this time. Reco the sum of Ra (autotrophic respiration) and Rh has been calculated as the difference of FluxSat GPP and GEOS-Chem NEE.

Deleted: suggest an



Deleted: The NEE flux presents a strong positive in June, followed by a gradual decrease up to October (monsoon).

1029 **Figure 7:** Monthly variation of atmospheric CO₂ mole fraction (for 2023) over the Sonipat
 1030 monitoring station compared against (a) biospheric fluxes from the MiCASA terrestrial
 1031 biospheric model and (b) GEOS-Chem model and FluxSat GPP data. (a - b) The CO₂ mole
 1032 fraction are daytime-mean (06:00 - 18:00 LT) and night time-mean (18:00 - 06:00 LT). The
 1033 correlation heatmap of all the variables. The annual growth rate of CO₂ has been subtracted
 1034 from the CO₂ mole fraction using background data from the Mauna Lou observatory. The
 1035 variable “Reco calc” was calculated as the difference between NEE (GEOS-Chem) and GPP
 1036 (FluxSat). The Pearson correlation coefficients with a p value less than 0.05 have been
 1037 displayed in the correlation plot.

1038
 1039 The NEE flux shows a strong positive in June, followed by a gradual decrease through
 1040 October (monsoon). During this time, Reco, Rh and GPP exhibit strong enhancements. These
 1041 enhancements are accompanied by a drawdown of CO₂ during this time. The driving factor
 1042 behind this CO₂ drawdown during monsoon is the enhanced ecosystem productivity during this
 1043 time. Strong inverse correlations of GPP, Rh, and Reco with CO₂ suggested that the biosphere
 1044 acts as a net sink of CO₂ (Figure 8c).

1045 Interestingly, post-monsoon and winter months exhibit weak or negative NEE. This is
 1046 because Rh values are low during these seasons due to drier soil conditions and lower soil
 1047 moisture. It is also notable that GPP is very low during these months, which is associated with
 1048 a high CO₂ mole fraction. Significant contributions of air-mass transport from upwind regions
 1049 and boundary-layer dynamics, along with the lack of vegetation during this time, contribute to
 1050 the buildup of CO₂ mole fraction.

1051
 1052

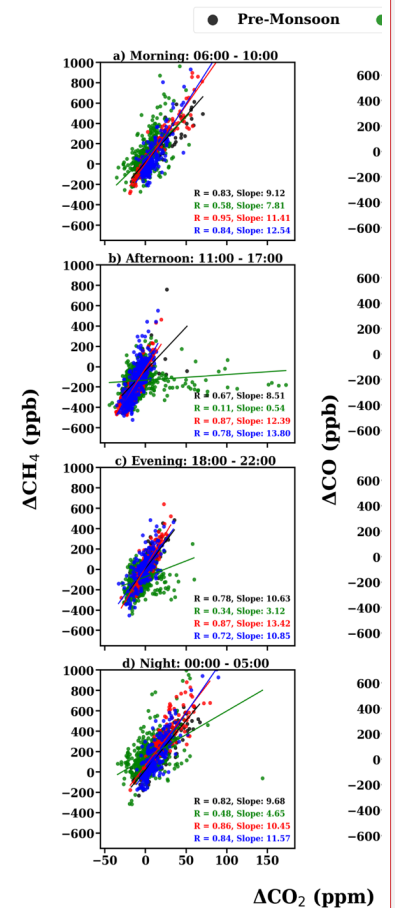
Moved down [7]: During this time, Reco, Rh and GPP exhibit strong enhancements. These enhancements are accompanied by

Moved down [8]: Interestingly, post-monsoon and winter months exhibit weak or negative NEE.

Deleted: the drawdown of CO₂ during this time. The driving factor for this drawdown of CO₂ during monsoon is the enhanced ecosystem productivity during this time.

Deleted: This is because the Rh values are low during these seasons due to the drier soil conditions and the lack of soil moisture. It is also notable that GPP is very low during these months, which is associated with high CO₂ mole fraction as well. This increase in mole fraction is not only due to the lack of vegetation but also due to contributions from other local sources as well. ¶ ... [41]

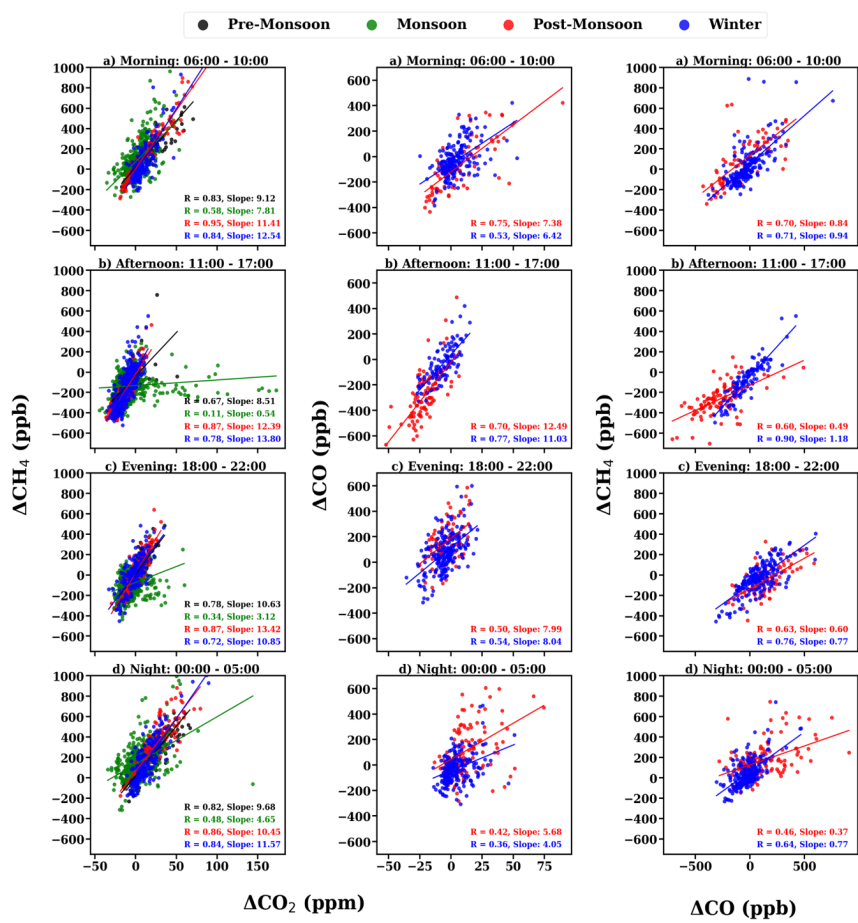
Formatted: Indent: First line: 0 cm



Deleted: ... [42]

Moved (insertion) [7]

Moved (insertion) [8]



1087
 1088 **Figure 8:** Tracer-tracer relations of $\Delta\text{CO}_2/\Delta\text{CH}_4$ (left panel), $\Delta\text{CO}_2/\Delta\text{CO}$ (middle panel) and
 1089 $\Delta\text{CH}_4/\Delta\text{CO}$ (right panel) during a) Morning (0600–1000 IST), b) afternoon (1100–1700 IST),
 1090 c) evening (1800–2200 IST) and d) night (0000–0500 IST).

1092 **3.5 Emission source detection using tracer-tracer relationships**

1093 The ratios (tracer-tracer) of GHGs have been widely used in previous studies to estimate
 1094 different emission source contributions to atmospheric GHGs (Chandra et al., 2016, 2019; Lin
 1095 et al., 2015; Lopez, 2012; Paris et al., 2008; Sreenivas et al., 2016, 2022). We followed a similar
 1096 tracer-tracer correlation analysis to assess synoptic variation in CO_2 across different diurnal
 1097 time windows and understand the emission sources contributing to CO_2 mole fractions over

- Deleted: 3.5 Tracer-Tracer
- Deleted: follow
- Deleted: though the stations are in different geographical locations, however this will help
- Deleted: the
- Deleted: of
- Deleted: at
- Deleted: to
- Deleted: fraction

1107 Sonipat (Figure 8). The measurements have been divided into four-time windows: (a) morning
1108 hours (06:00 - 10:00; the PBLH starts to develop after sunrise; local traffic is high), (b)
1109 afternoon hours (11:00 - 17:00; the PBLH is well-developed; relatively minimum local traffic,
1110 (c) evening hours (18:00 - 22:00; rush hour traffic and high household emissions), and (d) night
1111 hours (00:00 - 00:05; relatively less anthropogenic emission sources). Excess mole fractions
1112 were used in the correlation analysis to remove the influence of background mole fractions on
1113 the correlation ratios (Worthy et al., 2009). The correlation between the different gases (CO₂,
1114 CH₄, and CO) has been studied using the robust linear fit regression method.

1115
1116 Figure 8 (left panel) presents the correlation of excess mole fraction of CH₄ and CO₂
1117 during the four seasons. The CH₄/CO₂ correlation reveals a strong correlation ($r > 0.6$) for all
1118 seasons except monsoon during all time windows, which suggests a similar source mechanism
1119 or a controlling emission process for both gases at the measurement site. Around the monitoring
1120 station, vehicular emissions from the nearby highway and natural gas combustion emissions
1121 are possible sources. Also, a positive correlation suggests that anthropogenic emissions
1122 dominate the carbon cycle in Sonipat (Fang et al., 2015). The regression slope shows strong
1123 diurnal variation throughout all seasons. Recent studies across India have reported similar
1124 results, with higher regression slopes during the post-monsoon and winter seasons than during
1125 the pre-monsoon and monsoon seasons (Lin et al., 2015; Sreenivas et al., 2016, 2022).

1126
1127 Figure 8 (middle panel) presents the correlation of excess mole fractions of CO and
1128 CO₂ during post-monsoon and winter. The CO/CO₂ ratio over Sonipat (4 – 12.5 ppb ppm⁻¹) is
1129 lower than that for fresh plumes from wildfire (Andreae and Merlet, 2001; Mauzerall et al.,
1130 1998) and much lower than that from biomass burning events alone (Matsueda et al., 1999).
1131 Lin et al. (2015) reported CO/CO₂ ratios of 13 ppb ppm⁻¹ over Southeast Asian outflow from
1132 February to April 2001. This value was found to be influenced by fossil fuel emissions (Russo
1133 et al., 2003), crop residue burning, and biofuel burning rather than solely by biomass/biofuel
1134 burning. The CO/CO₂ ratios over Sonipat during the post-monsoon and winter closely match
1135 those of Lin et al. (2015), suggesting that the high CO₂ mole fractions during this time are an
1136 interplay of different sources like crop residue burning (long-range transport) and other fossil-
1137 fuel emissions (vehicular and industrial) around the monitoring station.

1138
1139 Figure 8 (right panel) presents the correlation of excess mole fractions of CH₄ and CO during
1140 post-monsoon and winter. The CH₄/CO ratios range from 0.3 to 1.2 at Sonipat, indicative of

Deleted: Fig. 9

Deleted: Excessive

Deleted: fraction

Deleted: fraction

Formatted: Indent: Left: 0.16 cm, First line: 0 cm

Deleted: 3.5.1 Correlation between CO₂ and CH₄

Deleted: 9

Deleted: study location

Deleted: the dominance of

Deleted: on

Deleted: over

Deleted: During monsoon season, the afternoon time window has a weak correlation with other time windows, revealing the different source and sink mechanisms of CO₂ and CH₄, such as the loss of CH₄ by hydroxyl radical and the uptake of CO₂ by plants. The regression slope exhibits a higher slope during the post-monsoon and winter months, and this is associated with...

Deleted: Similar

Deleted: presented

Deleted: high

Deleted: in comparison to

Deleted: 3.5.2 Correlation between CO₂ and CO

Deleted: 9

Deleted: fraction

Deleted: seasons. The CO/CO₂ correlation shows strong...

Formatted: Not Superscript/ Subscript

Deleted: those

Deleted: . The low ratios of CO/CO₂ can also be due to...

Formatted: Not Superscript/ Subscript

Deleted: suggested

Deleted: not only due to biomass/biofuel burning but also...

Deleted: have a combined influence on

Deleted: and CO mole fraction

Deleted:

Deleted: . Although there is a contribution

Deleted: CO and

Deleted: from long-range air mass transport (influence of

Formatted: Not Superscript/ Subscript

Deleted: over Punjab) from the northwest side of

Deleted: , the effect is diluted by other sources. Figure...

Formatted: Font: Not Bold

Deleted: 3.5.3 Correlation between CH₄ and CO

Deleted: 9

Deleted: fraction

Deleted: seasons. The CH₄/CO correlation reveals a strong...

Deleted: over

1222 anthropogenic emission sources (Bakwin et al., 1995; Harriss et al., 1994; Lai et al., 2010; Lin
 1223 et al., 2015; Niwa et al., 2012; Sawa et al., 2004; Wada et al., 2011; Xiao et al., 2004). In
 1224 contrast, ratios influenced solely by biomass and biofuel burning are much lower, ranging from
 1225 0.07 to 0.3 (Andreae and Merlet, 2001; Mauzerall et al., 1998; Mühle et al., 2002).

1226 These lower ratios highlight the significant difference when compared to the values
 1227 recorded in Sonipat. Moreover, very high CH₄ emissions from livestock can elevate the
 1228 generally low CH₄/CO ratios associated with biomass burning. This indicates substantial
 1229 contributions from various CH₄ sources apart from biofuel burning.

Deleted: The CH₄/CO

Deleted: range of 0.07 – 0.3 indicates the contribution from

Deleted: Lin et al. (2015) presented similar

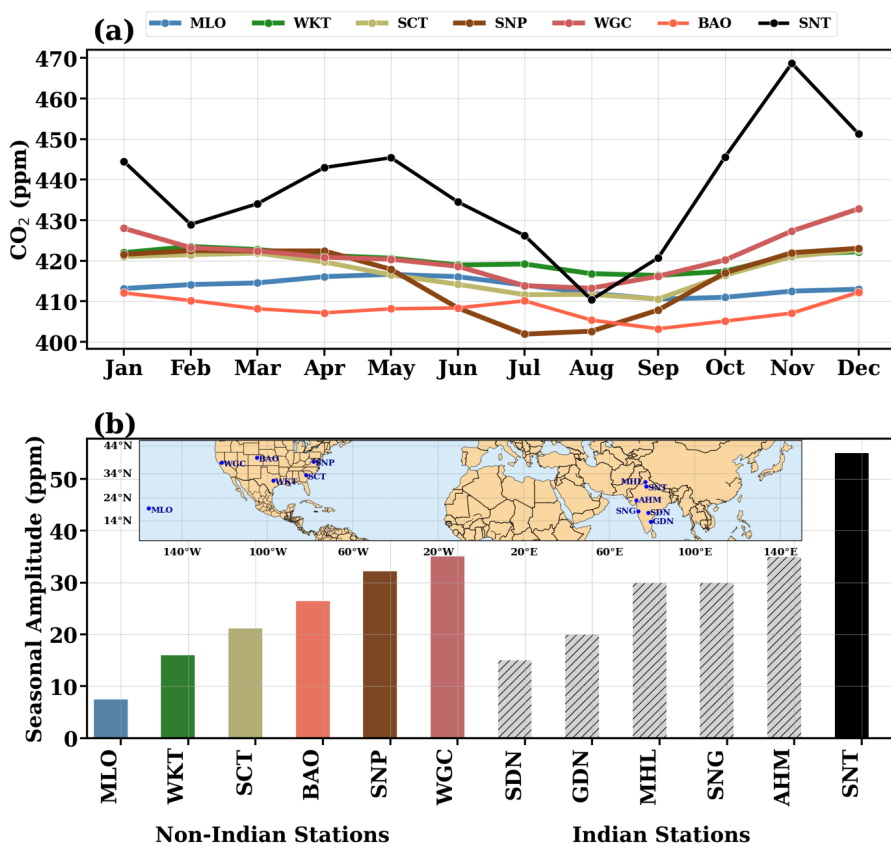
Deleted: of CH₄/CO over Pondicherry (PON) and Port Blair (PBL). High

Deleted: raise

Deleted: from

Deleted: CH₄ and CO emissions from biomass,

Deleted: and livestock estimated from EDGAR v4.2, 2011 indicate a CH₄/CO ratio of 0.64 – 0.69 over the Indian subcontinent from 2000-2008. These ratios are comparable to the ratios observed during both seasons over Sonipat.



1231 **Figure 9:** (a) Comparison of the seasonal variability of atmospheric CO₂ over Sonipat
 1232 monitoring station with various locations in the same latitudinal band. (b) Comparison of the
 1233 seasonal amplitude between Indian (coloured bars) and international monitoring stations (grey
 1234 bars). Indian stations include Shadnagar (SDN), Sinhadag (SNG), Ahmedabad (AHM), Mohali
 1235

Moved (insertion) [3]

1248 (MHL), Gadanki (GDN), and Sonipat (SNT). International stations include Mauna Loa (MLO),
1249 South Carolina (SCT), Shenandoah National Park (SNP), Walnut Grove, (WGC), Moody
1250 (WKT) and Boulder (BAO). For all international stations except BAO, the five-year average
1251 (2018 - 2022) has been chosen for the seasonality. For BAO, 2011 – 2016 has been used due
1252 to lack of coinciding data. The monthly average of the entire study period (February 2023 –
1253 January 2025) has been used for this comparison.

1254 **4. Discussions**

1256 By investigating two years of high-frequency atmospheric CO₂ mole fraction measurements at
1257 the Sonipat station in the IGP region, we identified the following salient features about the
1258 seasonality, diurnal variability, drivers of temporal variability, and emission sources of CO₂.

1259 **Very high atmospheric CO₂ mole fractions over IGP:** The surface-based
1260 measurements of atmospheric CO₂ mole fraction exhibit strong seasonality, with a maximum
1261 (456.4 ppm) during post-monsoon and a minimum (407.2 ppm) during monsoon, with an
1262 average of 422.6 ppm. Seasonal changes in the PBLH affected the atmospheric CO₂ mole
1263 fraction by diluting or concentrating GHG mole fractions near the surface. A strong dependence
1264 of CO₂ seasonality on local vegetative carbon uptake was observed from the negative
1265 correlation between NDVI and CO₂ mole fractions, which was consistent across India (Metya
1266 et al., 2021; Sreenivas et al., 2016; Tiwari et al., 2014).

1267 A comparison of the seasonality of atmospheric CO₂ at Sonipat with other Indian and
1268 global sites in the same latitudinal band revealed very high seasonality at Sonipat, surpassing
1269 that of all other stations. This high seasonality is attributed to elevated CO₂ mole fractions in
1270 November (post-monsoon), driven by local emissions and crop residue burning. Figure 9a
1271 presents the monthly averaged variation of CO₂ over Sonipat during the study period (SNT)
1272 with other measurement sites in the same latitudinal band (5° N – 40° N). Details of all
1273 monitoring stations used in this study are described in detail in S1. Sonipat exhibits a very high
1274 seasonal amplitude (~60 ppm) compared to other sites worldwide (~15 ppm, see Figure 9b),
1275 attributed to the sharp increase in post-monsoon, consistent in both years of the study (see
1276 Figure 2). Excluding November would reduce the seasonal amplitude of Sonipat to 35 ppm,
1277 which is comparable to that in Ahmedabad (35 ppm). Temperature-driven PBLH (which
1278 inhibits mixing) and strong north-westerly winds (which induce transport of emissions from
1279 upwind) during this season play a key role in these high CO₂ mole fractions (Figure S2 and

Moved down [9]: Conclusions ¶

Deleted: ¶
4.

Moved (insertion) [4]

Formatted: Font: Bold

Deleted: This study investigated the high temporal variability of atmospheric CO₂ mole fraction at Sonipat, a suburban station in the Indo-Gangetic Plain. Sonipat's location, being in the downwind of Punjab and upwind of Delhi, makes it an ideal site for examining the influence of different regional air masses in the IGP region. The atmospheric CO₂ mole fraction from February 2023 to January 2025 have been measured with a GHG analyser using the laser-based cavity ring-down spectroscopy technique. To understand the key drivers of seasonal and diurnal CO₂ variability over the Sonipat station and the IGP region, we used a combination of ground-based and satellite-based measurements, three different model outputs, ecosystem proxy variables, and tracer-tracer analysis technique. ¶

The salient findings from this study are listed below. ¶
The surface-based measurements of atmospheric CO₂ mole fraction exhibit the large CO₂ seasonality with maximum mole fraction (456.4 ppm) during post-monsoon and minimum mole fraction (407.2 ppm) during monsoon, with an average mole fraction of 422.6 ppm. ¶
The comparison of the seasonality of atmospheric CO₂ over Sonipat...

Formatted: Indent: First line: 1.27 cm, Space Before: 12 pt, After: 12 pt, No bullets or numbering

Deleted: reveals

Deleted: over that is observed

Deleted: the high

Deleted: fraction of CO₂ during

Deleted:) from

Deleted: The location of the

Deleted: site

Deleted: IGP region on the downwind

Deleted: Punjab is a major reason for

Deleted: strong

Deleted: variability

Deleted: in the same latitudinal band. ¶
Our results also indicate that the biospheric activity was the primary driver of CO₂ seasonal variability over Sonipat, with anthropogenic emissions and soil respiration as the major sources and photosynthetic carbon uptake as the major sink. In addition, the boundary layer dynamics and air mass transport

Deleted: regions significantly contribute to the build-up of

Deleted: fraction.

1325 S3). It is also noted that the CO₂ drawdown in August is primarily due to the green paddy fields
1326 during the monsoon (terrestrial CO₂ uptake), coinciding with heavy rains that wash out CO₂.
1327 This combined effect makes the lowest CO₂ mole fractions in Sonipat comparable to those at
1328 some background stations across the globe with different ecosystems (Figure 9a).

1329 This study also analysed the drivers of this variability using various ecosystem variables,
1330 including NEE, which represents the net carbon exchange between terrestrial ecosystems (the
1331 difference between Rh and NPP). NPP is the net amount of CO₂ retained in the biosphere. Rh
1332 is the amount of CO₂ emitted into the atmosphere due to the decomposition of organic matter
1333 by microorganisms in the soil. Reco, the sum of Ra (autotrophic respiration) and Rh has been
1334 calculated as the difference of FluxSat GPP and GEOS-Chem NEE. GPP, a measure of carbon
1335 uptake by plants, was observed to be very high during monsoon along with NEE, Rh and Reco.
1336 Statistical analysis revealed a strong negative correlation of GPP with CO₂ and a strong positive
1337 correlation with Rh and Reco. These suggest that the primary sink of CO₂ over Sonipat is
1338 biospheric activity, driven by the abundance of vegetation resulting from enhanced soil
1339 moisture during the monsoon.

1340 **Performance of models and satellites over IGP:** Although both the CarbonTracker
1341 and MIROC-ACTM models captured the broad seasonal pattern of CO₂ mole fractions, they
1342 substantially underestimated it. However, MIROC showed greater seasonal variability than
1343 CT2022, with post-monsoon highs and pre-monsoon drawdowns showing strong correlations
1344 with in situ measurements. Further analysis of the tracers from MIROC provides insights into
1345 the driving factors of this variability. The post-monsoon peak is attributed to vehicular
1346 emissions from the nearby highway and industrial sources upwind of the monitoring station.
1347 The drawdown in monsoon is attributed to the added soil moisture and increased CO₂ uptake
1348 by plants during this time. The location of the measurement site in IGP, downwind of Punjab,
1349 provides insights into this transport-induced enhancement. The OCO-2 and OCO-3 satellite
1350 XCO₂ retrievals also showed similar seasonal variability; however, the satellites could not
1351 capture CO₂ enhancements from local sources.

1352 **Diurnal variability driven by meteorology:** The atmospheric CO₂ mole fraction at
1353 Sonipat exhibits a consistent diurnal pattern across seasons. It was observed that CO₂ mole
1354 fractions steadily increased throughout the night, reaching a peak in the early morning hours.
1355 This accumulation of CO₂ during the night-time can be attributed to the fumigation effect; a
1356 significant rise in surface mole fractions, notable during the early morning hours due to the

Moved (insertion) [6]

Formatted: Indent: First line: 1.27 cm, No bullets or numbering

Deleted: could capture

Deleted: fraction, the models

Deleted: the CO₂ mole fraction.

Deleted: revealed

Deleted: due to

Deleted: exhibit

Deleted: irrespective of season, with an

Deleted: maximum during

Deleted: , which

Deleted: , with a gradual decrease during the day and a minimum during afternoon hours with enhanced

1368 breakdown of the nocturnal inversion layer following sunrise (Stull, 1988). Weak winds and
1369 shallow PBLH enhance the fumigation effect. The combined effect of photosynthetic activity
1370 and mixing of PBLH during the afternoon hours drives the CO₂ mole fractions during different
1371 seasons. The diurnal amplitude shows large month-to-month variation with an increasing trend
1372 from May to September 2023 and a decreasing trend till February 2024. Figure S5 presents the
1373 seasonal variation of CO₂ compared with PBLH derived from Ceilometer and ERA5 reanalysis
1374 data for 2023. A slight shift in the timing of the morning peaks was observed from season to
1375 season, due to changes in sunrise time, which affected photosynthetic activity.

1376 **Detecting emission source contributions:** Tracer-tracer relationships across different
1377 time periods during the post-monsoon and winter seasons were examined. Analysis reveals
1378 that CO₂ and CH₄ exhibit a strong positive correlation across all seasons, suggesting common
1379 sources for both gases. During monsoon season, the afternoon time window shows a weak
1380 correlation with other time windows, revealing distinct source and sink mechanisms for CO₂
1381 and CH₄, such as CH₄ loss via hydroxyl radical and CO₂ uptake by plants. The regression
1382 slope is higher during the post-monsoon and winter months, when reduced photosynthetic
1383 activity and the dominance of local emissions and long-range transport are observed. The
1384 lower values during pre-monsoon and monsoon are associated with the dominance of
1385 vegetation and terrestrial uptake of CO₂ by photosynthetic activity.

1386 The CO/CO₂ correlation shows strong diurnal variability, suggesting the dominance of
1387 different source mechanisms throughout the day, with strong correlation during the morning
1388 and afternoon hours (suggesting a similar source) and weaker correlation during the evening
1389 and night hours (suggesting different sources). The post-monsoon season shows higher
1390 regression slopes due to reduced photosynthetic activity. Over Sonipat, the contribution of CO
1391 and CO₂ from long-range airmass transport (influenced by crop residue burning in Punjab)
1392 during post-monsoon from the northwest of the monitoring station is diluted by other sources
1393 (such as vehicular emissions from highways, crop residue burning, and open burning). The
1394 contribution of biofuel burning (which has a higher burning efficiency) during post-monsoon
1395 and winter (Andreae and Merlet, 2001) can also reduce the CO/CO₂ ratios. Figure S2 presents
1396 the wind patterns during the different seasons, revealing the predominant winds from the
1397 northwest during the post-monsoon season. The CO/CO₂ ratios reveal the combined influence
1398 of various sources around and upwind of the monitoring station during the post-monsoon
1399 period.

Moved (insertion) [5]

Deleted: .

Deleted: time for

Deleted: the change

Deleted: the time of

Deleted: , resulting in a shift in

Deleted: The diurnal amplitude of CO₂ was observed to peak in post-monsoon (maximum in November) and draw down (minimum in May) in monsoon.

Deleted: The tracer

Deleted: during

Deleted: for

Deleted: show a strong positive correlation during all seasons, and the higher slopes are due to the lack of

Formatted: Not Superscript/ Subscript

Formatted: Not Superscript/ Subscript

Deleted: influence of local winds. This strong correlation suggests common anthropogenic sources for both these gases. The CO/CO₂ ratios reveal the influence of

Deleted: of

Formatted: Indent: First line: 1.27 cm, No bullets or numbering

Deleted: over Punjab on CO₂ mole fraction in Sonipat during post-monsoon.

.....Page Break.....

Formatted: Font: Not Bold

1420 The CH₄/CO correlation ($r > 0.7$) was stronger during winter than during post-monsoon
1421 across all time windows, suggesting similar sources during winter and different sources during
1422 post-monsoon. The regression slope was higher during winter than during the post-monsoon
1423 period. This was traced to the lack of photosynthetic activity and the dominance of local
1424 emissions and long-range transport. Lin et al. (2015) reported comparable CH₄/CO ratios at
1425 Pondicherry (PON) and Port Blair (PBL). CH₄ and CO emissions from biomass, biofuel
1426 burning and livestock estimated from EDGAR v4.2, 2011 indicate a CH₄/CO ratio of 0.64 –
1427 0.69 over the Indian subcontinent from 2000-2008. These ratios are comparable to those
1428 observed during both seasons at Sonipat.

1429 In summary, this study demonstrated that this high temporal CO₂ variability across the
1430 IGP region arises from an interplay of local anthropogenic and biomass-burning emissions,
1431 biospheric fluxes, and prevailing meteorology.

1432 5. Conclusions

1433 In this study, we conducted high frequency measurements of atmospheric CO₂ mole fractions
1434 at a suburban station in the Indo-Gangetic Plain, Sonipat and investigated the carbon cycle
1435 dynamics over IGP. The atmospheric CO₂ mole fractions from February 2023 to January 2025
1436 have been measured using a GHG analyser with laser-based cavity ring-down spectroscopy.
1437 CO₂ molefractions over Sonipat recorded an annual average of 440.8±19.7 parts per million
1438 (ppm) in 2024, with a very high seasonal variability of ~60 ppm, much higher than that of other
1439 monitoring stations in the same latitudnal band. Post-monsoon recorded the highest diurnal
1440 variability (~ 60 ppm) and monsoon recorded the least (~20 ppm) with a consistent diurnal
1441 pattern irrespective of season. By examining a series of observational and modelling data, such
1442 as ground-based and satellite-based measurements, three model outputs, ecosystem proxy
1443 variables, and the tracer-tracer analysis technique, we identified the drivers of the high temporal
1444 variability of CO₂ over Sonipat and the IGP region. First, this high seasonality is attributed to
1445 elevated CO₂ mole fractions in November (post-monsoon), driven by local emissions and crop
1446 residue burning. We found that biospheric activity was the primary driver of seasonal changes
1447 over Sonipat, with anthropogenic emissions and soil respiration as the major sources and
1448 photosynthetic carbon uptake as the major sink. In addition, boundary-layer dynamics and air-
1449 mass transport from upwind regions significantly contribute to the buildup of CO₂ mole
1450 fraction. Second, we found that although both the CarbonTracker and MIROC-ACTM models
1451 captured the broad seasonal pattern of CO₂ mole fractions, they substantially underestimated
1452 it. Moreover, the OCO-2 and OCO-3 satellite XCO₂ retrievals also showed similar seasonal
1453 it.

Moved (insertion) [9]

1454 variability; however, the satellites could not capture CO₂ enhancements from local sources.
1455 Third, we found that the atmospheric CO₂ mole fraction at Sonipat exhibits a consistent diurnal
1456 pattern irrespective of season, with a maximum during the morning hours, attributed to the
1457 fumigation effect, followed by a gradual decrease during the day and a minimum during the
1458 afternoon hours, when photosynthetic activity is enhanced. Finally, tracer-tracer relationships
1459 across different time periods in the post-monsoon and winter seasons revealed common sources
1460 of CO₂ and CH₄. The CO/CO₂ ratios reveal the combined influence of vehicular emissions,
1461 crop residue burning, and open burning on CO₂ mole fractions in Sonipat during the post-
1462 monsoon period. This study identified key sources and drivers of the high CO₂ temporal
1463 variability in a data-sparse IGP region. These findings advance our understanding of carbon
1464 cycle dynamics, with direct implications for mitigation and policy.

1465 Data availability

- 1466 • The OCO-2 and OCO-3 data is downloaded from <https://disc.gsfc.nasa.gov/datasets/>.
1467 This study utilizes the bias-corrected OCO-2 v11.1r data product
1468 (https://disc.gsfc.nasa.gov/datasets/OCO2_L2_Lite_FP_11.1r/summary?keywords=oco2) and the OCO-3 v10.4r data product
1469 (https://disc.gsfc.nasa.gov/datasets/OCO3_L2_Lite_FP_10.4r/summary?keywords=oco3).
- 1472 • The CT-2020 model outputs were downloaded from
1473 <https://gml.noaa.gov/aftp/products/carbontracker/co2/>. The CASA model outputs
1474 were downloaded from
1475 https://disc.gsfc.nasa.gov/datasets/GEOS_CASAGFED_M_FLUX_3/summary?keywords=CASA.
- 1477 • The ERA5 reanalysis datasets were downloaded from
1478 <https://cds.climate.copernicus.eu/cdsapp#!/dataset/reanalysis-era5-single-levels>.
- 1479 • The satellite estimates of NDVI were downloaded from
1480 <https://www.ncei.noaa.gov/data/land-normalized-difference-vegetation-index/access/>.
- 1481 • This study utilises bias-corrected SIF data from OCO-2 v11r data product
1482 (https://disc.gsfc.nasa.gov/datasets/OCO2_L2_Lite_SIF_11r/summary?keywords=oco2%20sif).
- 1484 • The FluxSat data is downloaded from
1485 https://avdc.gsfc.nasa.gov/pub/tmp/FluxSat_GPP/. This study uses FluxSat version
1486 2.2 dataproduct.

Formatted: Font colour: Black

Formatted: Normal, Outline numbered + Level: 1 +
Numbering Style: Bullet + Aligned at: 0.63 cm + Indent at:
1.27 cm, Border: Top: (No border), Bottom: (No border),
Left: (No border), Right: (No border), Between : (No border)

Formatted: Font colour: Black

Formatted: Font colour: Black

Formatted: Font colour: Black

Formatted: Font colour: Black

Deleted: <https://cds.climate.copernicus.eu/cdsapp#!/dataset/reanalysis-era5-single-levels>.

Formatted: Font colour: Black

Formatted: Font colour: Black

Deleted: <https://www.ncei.noaa.gov/data/land-normalized-difference-vegetation-index/access/>.

Formatted: Font colour: Black

Formatted: Font colour: Black

Deleted: https://disc.gsfc.nasa.gov/datasets/OCO2_L2_Lite_SIF_11r/summary?keywords=oco2%20sif

Formatted: Font colour: Black

Formatted: Font colour: Black

Deleted: https://avdc.gsfc.nasa.gov/pub/tmp/FluxSat_GPP/
....

Formatted: Font colour: Black

1495 • The ObsPack data is available at <https://gml.noaa.gov/ccgg/obspack/data.php>. This
1496 study used ObsPack V2.0 dataproduct.

Deleted: <https://gml.noaa.gov/ccgg/obspack/data.php>.

Formatted: Font colour: Black

Formatted: Font colour: Black

Deleted: ¶

Formatted: Font: Not Bold

1497
1498 **Acknowledgements:**

1499 We acknowledge institutional support and funding provided by IIT Delhi and other
1500 stakeholders to develop the IIT Delhi Atmospheric Observatory at Sonipat. In particular, we
1501 thank Shahzad Gani (IIT Delhi) for his contribution to the observatory. We thank the Aakash
1502 Project team for providing trace gas data from the CUPI-G sensors. We acknowledge the OCO-
1503 2, OCO-3, CASA, CarbonTracker, and ERA5 teams for providing the data used in this study.

1504
1505
1506 **Author Contributions:**

1507 **Conceptualization:** VJV, RKK, SP

1508 **Data curation:** VJV, RKK, JR, DG, SD, YM, PKP

1509 **Investigation, Methodology:** VJV, RKK, SP, PKP

1510 **Software, Visualisation:** VJV

1511 **Writing – original draft:** VJV

1512 **Writing – review & editing:** RKK, [SP](#), JR, DG, SD, YM, PKP

1513
1514 **Competing interests**

1515 The authors declare that they have no conflict of interest.

Formatted: Justified, Space After: 10 pt

1518 **References**

1519 [Aburas, M. M., Abdullah, S. H., Ramli, M. F., and Ash'aari, Z. H.: Measuring Land Cover](#)
 1520 [Change in Seremban, Malaysia Using NDVI Index, *Procedia Environmental Sciences*, 30,](#)
 1521 [238–243, <https://doi.org/10.1016/j.proenv.2015.10.043>, 2015.](#)

1522 [Ammoura, L., Xueref-Remy, I., Gros, V., Baudic, A., Bonsang, B., Petit, J.-E., Perrussel, O.,](#)
 1523 [Bonnaire, N., Sciare, J., and Chevallier, F.: Atmospheric measurements of ratios between](#)
 1524 [CO₂ and co-emitted species from traffic: a tunnel study in the Paris](#)
 1525 [megacity, *Atmos. Chem. Phys.*, 14, 12871–12882, \[https://doi.org/10.5194/acp-\]\(https://doi.org/10.5194/acp-14-12871-2014\)](#)
 1526 [2014, 2014.](#)

1527 [Andreae, M. O. and Merlet, P.: Emission of trace gases and aerosols from biomass burning,](#)
 1528 [Global Biogeochemical Cycles, 15, 955–966, <https://doi.org/10.1029/2000GB001382>, 2001.](#)

1529 [Apadula, F., Cassardo, C., Ferrarese, S., Heltai, D., and Lanza, A.: Thirty Years of](#)
 1530 [Atmospheric CO₂ Observations at the Plateau Rosa Station, Italy, *Atmosphere*, 10, 418,](#)
 1531 [https://doi.org/10.3390/atmos10070418, 2019.](#)

1532 [Baars, H., Ansmann, A., Engelmann, R., and Althausen, D.: Continuous monitoring of the](#)
 1533 [boundary-layer top with lidar, *Atmospheric Chemistry and Physics*, 8, 7281–7296,](#)
 1534 [https://doi.org/10.5194/acp-8-7281-2008, 2008.](#)

1535 [Baker, A. K., Schuck, T. J., Brenninkmeijer, C. A. M., Rauthe-Schöch, A., Slemr, F., van](#)
 1536 [Velthoven, P. F. J., and Lelieveld, J.: Estimating the contribution of monsoon-related](#)
 1537 [biogenic production to methane emissions from South Asia using CARIBIC observations,](#)
 1538 [Geophysical Research Letters, 39, <https://doi.org/10.1029/2012GL051756>, 2012.](#)

1539 [Bakwin, P. S., Tans, P. S., Zhao, C., Ussler III, W., and Quesnell, E.: Measurements of](#)
 1540 [carbon dioxide on a very tall tower, *Tellus B: Chemical and Physical Meteorology*, 47, 535–](#)
 1541 [549, <https://doi.org/10.3402/tellusb.v47i5.16070>, 1995.](#)

1542 [Bhattacharya, S. K., Borole, D. V., Francy, R. J., Allison, C. E., Steele, L. P., Krummel, P.,](#)
 1543 [Langenfelds, R., Masarie, K. A., Tiwari, Y. K., and Patra, P. K.: Trace gases and CO₂ isotope](#)
 1544 [records from Cabo de Rama, India, *Current Science*, 97, 1336–1344, 2009.](#)

1545 [Bisht, J. S. H., Machida, T., Chandra, N., Tsuboi, K., Patra, P. K., Umezawa, T., Niwa, Y.,](#)
 1546 [Sawa, Y., Morimoto, S., Nakazawa, T., Saitoh, N., and Takigawa, M.: Seasonal Variations of](#)
 1547 [SF₆, CO₂, CH₄, and N₂O in the UT/LS Region due to Emissions, Transport, and Chemistry,](#)
 1548 [JGR Atmospheres, 126, e2020JD033541, <https://doi.org/10.1029/2020JD033541>, 2021.](#)

1549 [Brad Weir \(2024\), MiCASA Daily NPP Rh Fire Fuel Fluxes 0.1 degree × 0.1 degree V1,](#)
 1550 [Greenbelt, MD, USA, NASA Center for Climate Simulation \(NCCS\) DataPortal, Accessed:](#)
 1551 [\[March 20, 2025\], \[10.5067/ZBXSA1LEN453\]\(https://doi.org/10.5067/ZBXSA1LEN453\)](#)

1552 [Byrne, B., Jones, D. B. A., Strong, K., Zeng, Z., -C., Deng, F., and Liu, J.: Sensitivity of CO₂](#)
 1553 [surface flux constraints to observational coverage, *JGR Atmospheres*, 122, 6672–6694,](#)
 1554 [https://doi.org/10.1002/2016JD026164, 2017.](#)

1555 [Chakraborty, S., Tiwari, Y. K., Deb Burman, P. K., Baidya Roy, S., and Valsala, V.:](#)
 1556 [Observations and Modeling of GHG Concentrations and Fluxes Over India, in: Assessment](#)

Deleted: Aburas, M. M., Abdullah, S. H., Ramli, M. F., and Ash'aari, Z. H.: Measuring Land Cover Change in Seremban, Malaysia Using NDVI Index, *Procedia Environmental Sciences*, 30, 238–243, <https://doi.org/10.1016/j.proenv.2015.10.043>, 2015.

Ammoura, L., Xueref-Remy, I., Gros, V., Baudic, A., Bonsang, B., Petit, J.-E., Perrussel, O., Bonnaire, N., Sciare, J., and Chevallier, F.: Atmospheric measurements of ratios between CO₂ and co-emitted species from traffic: a tunnel study in the Paris megacity, *Atmos. Chem. Phys.*, 14, 12871–12882, <https://doi.org/10.5194/acp-14-12871-2014>, 2014.

Andreae, M. O. and Merlet, P.: Emission of trace gases and aerosols from biomass burning, *Global Biogeochemical Cycles*, 15, 955–966, <https://doi.org/10.1029/2000GB001382>, 2001.

Apadula, F., Cassardo, C., Ferrarese, S., Heltai, D., and Lanza, A.: Thirty Years of Atmospheric CO₂ Observations at the Plateau Rosa Station, Italy, *Atmosphere*, 10, 418, <https://doi.org/10.3390/atmos10070418>, 2019.

Baars, H., Ansmann, A., Engelmann, R., and Althausen, D.: Continuous monitoring of the boundary-layer top with lidar, *Atmospheric Chemistry and Physics*, 8, 7281–7296, <https://doi.org/10.5194/acp-8-7281-2008>, 2008.

Baker, A. K., Schuck, T. J., Brenninkmeijer, C. A. M., Rauthe-Schöch, A., Slemr, F., van Velthoven, P. F. J., and Lelieveld, J.: Estimating the contribution of monsoon-related biogenic production to methane emissions from South Asia using CARIBIC observations, *Geophysical Research Letters*, 39, <https://doi.org/10.1029/2012GL051756>, 2012.

Bakwin, P. S., Tans, P. S., Zhao, C., Ussler III, W., and Quesnell, E.: Measurements of carbon dioxide on a very tall tower, *Tellus B: Chemical and Physical Meteorology*, 47, 535–549, <https://doi.org/10.3402/tellusb.v47i5.16070>, 1995.

Bhattacharya, S. K., Borole, D. V., Francy, R. J., Allison, C. E., Steele, L. P., Krummel, P., Langenfelds, R., Masarie, K. A., Tiwari, Y. K., and Patra, P. K.: Trace gases and CO₂ isotope records from Cabo de Rama, India, *Current Science*, 97, 1336–1344, 2009.

Bisht, J. S. H., Machida, T., Chandra, N., Tsuboi, K., Patra, P. K., Umezawa, T., Niwa, Y., Sawa, Y., Morimoto, S., Nakazawa, T., Saitoh, N., and Takigawa, M.: Seasonal Variations of SF₆, CO₂, CH₄, and N₂O in the UT/LS Region due to Emissions, Transport, and Chemistry, *JGR Atmospheres*, 126, e2020JD033541, <https://doi.org/10.1029/2020JD033541>, 2021.

Brad Weir (2024), MiCASA Daily NPP Rh Fire Fuel Fluxes 0.1 degree × 0.1 degree V1, Greenbelt, MD, USA, NASA Center for Climate Simulation (NCCS) DataPortal, Accessed: [March 20, 2025], [10.5067/ZBXSA1LEN453](https://doi.org/10.5067/ZBXSA1LEN453)

Byrne, B., Jones, D. B. A., Strong, K., Zeng, Z., -C., Deng, F., and Liu, J.: Sensitivity of CO₂ surface flux constraints to observational coverage, *JGR Atmospheres*, 122, 6672–6694, <https://doi.org/10.1002/2016JD026164>, 2017.

Campbell, J. E., Carmichael, G. R., Chai, T., Mena-Carrasco, M., Tang, Y., Blake, D. R., Blake, N. J., Vay, S. A., Collatz, G. J., Baker, I., Berry, J. A., Montzka, S. A., Sweeney, C., Schnoor, J. L., and Stanier, C. O.: Photosynthetic Control of Atmospheric Carbonyl Sulfide During the Growing Season, *Science*, 322, 1085–1088, <https://doi.org/10.1126/science.1164015>, 2008.

Chakraborty, S., Tiwari, Y. K., Deb Burman, P. K., Baidya Roy, S., and Valsala, V.: Observations and Modeling of GHG Concentrations and Fluxes Over India, in: Assessment of Climate Change over the Indian Region: A Report of the Ministry of Earth Sciences (MoES), Government of India, edited by: Krishnan, R., Sanjay, J., Gnanaseelan, C., ... [49]

1705 [of Climate Change over the Indian Region: A Report of the Ministry of Earth Sciences](#)
1706 [\(MoES\), Government of India, edited by: Krishnan, R., Sanjay, J., Gnanaseelan, C.,](#)
1707 [Mujumdar, M., Kulkarni, A., and Chakraborty, S., Springer, Singapore, 73–92,](#)
1708 https://doi.org/10.1007/978-981-15-4327-2_4, 2020.

1709 [Chandra, N., Lal, S., Venkataramani, S., Patra, P. K., and Sheel, V.: Temporal variations of](#)
1710 [atmospheric CO₂ and CO at Ahmedabad in western India, Atmos.](#)
1711 [Chem. Phys., 16, 6153–6173, https://doi.org/10.5194/acp-16-6153-2016](#), 2016.

1712 [Chandra, N., Venkataramani, S., Lal, S., Patra, P. K., Ramonet, M., Lin, X., and Sharma, S.](#)
1713 [K.: Observational evidence of high methane emissions over a city in western India,](#)
1714 [Atmospheric Environment, 202, 41–52, https://doi.org/10.1016/j.atmosenv.2019.01.007,](#)
1715 [2019.](#)

1716 [Chandra, N., Patra, P. K., Bisht, J. S. H., Ito, A., Umezawa, T., Saigusa, N., Morimoto, S.,](#)
1717 [Aoki, S., Janssens-Maenhout, G., Fujita, R., Takigawa, M., Watanabe, S., Saitoh, N., and](#)
1718 [Canadell, J. G.: Emissions from the Oil and Gas Sectors, Coal Mining and Ruminant Farming](#)
1719 [Drive Methane Growth over the Past Three Decades, Journal of the Meteorological Society](#)
1720 [of Japan, 99, 309–337, https://doi.org/10.2151/jmsj.2021-015](#), 2021.

1721 [Chandra, N., Patra, P. K., Niwa, Y., Ito, A., Iida, Y., Goto, D., Morimoto, S., Kondo, M.,](#)
1722 [Takigawa, M., Hajima, T., and Watanabe, M.: Estimated regional CO₂ flux and uncertainty](#)
1723 [based on an ensemble of atmospheric CO₂ inversions, Atmos. Chem. Phys., 22, 9215–9243,](#)
1724 <https://doi.org/10.5194/acp-22-9215-2022>, 2022.

1725 [Chen, H., Karion, A., Rella, C. W., Winderlich, J., Gerbig, C., Filges, A., Newberger, T.,](#)
1726 [Sweeney, C., and Tans, P. P.: Accurate measurements of carbon monoxide in humid air using](#)
1727 [the cavity ring-down spectroscopy \(CRDS\) technique, Atmospheric Measurement](#)
1728 [Techniques, 6, 1031–1040, https://doi.org/10.5194/amt-6-1031-2013](#), 2013.

1729 [Chen, Y., Hall, J., Van Wees, D., Andela, N., Hantson, S., Giglio, L., Van Der Werf, G. R.,](#)
1730 [Morton, D. C., and Randerson, J. T.: Multi-decadal trends and variability in burned area from](#)
1731 [the fifth version of the Global Fire Emissions Database \(GFED5\), Earth Syst. Sci. Data, 15,](#)
1732 [5227–5259, https://doi.org/10.5194/essd-15-5227-2023](https://doi.org/10.5194/essd-15-5227-2023), 2023.

1733 [Crisp, D., Pollock, H. R., Rosenberg, R., Chapsky, L., Lee, R. A. M., Oyafuso, F. A.,](#)
1734 [Frankenberg, C., O'Dell, C. W., Bruegge, C. J., Doran, G. B., Eldering, A., Fisher, B. M., Fu,](#)
1735 [D., Gunson, M. R., Mandrake, L., Osterman, G. B., Schwandner, F. M., Sun, K., Taylor, T.](#)
1736 [E., Wennberg, P. O., and Wunch, D.: The on-orbit performance of the Orbiting Carbon](#)
1737 [Observatory-2 \(OCO-2\) instrument and its radiometrically calibrated products, Atmos. Meas.](#)
1738 [Tech., 10, 59–81, https://doi.org/10.5194/amt-10-59-2017](#), 2017.

1739 [Das, C., Kunchala, R. K., Chandra, N., Chhabra, A., and Pandya, M. R.: Characterizing the](#)
1740 [regional XCO₂ variability and its association with ENSO over India inferred from GOSAT](#)
1741 [and OCO-2 satellite observations, Science of The Total Environment, 902, 166176,](#)
1742 <https://doi.org/10.1016/j.scitotenv.2023.166176>, 2023.

1743 [Eldering, A., O'Dell, C. W., Wennberg, P. O., Crisp, D., Gunson, M. R., Viatte, C., Avis, C.,](#)
1744 [Braverman, A., Castano, R., Chang, A., Chapsky, L., Cheng, C., Connor, B., Dang, L.,](#)
1745 [Doran, G., Fisher, B., Frankenberg, C., Fu, D., Granat, R., Hobbs, J., Lee, R. A. M.,](#)
1746 [Mandrake, L., McDuffie, J., Miller, C. E., Myers, V., Natraj, V., O'Brien, D., Osterman, G.](#)

1747 B., Oyafuso, F., Payne, V. H., Pollock, H. R., Polonsky, I., Roehl, C. M., Rosenberg, R.,
1748 Schwandner, F., Smyth, M., Tang, V., Taylor, T. E., To, C., Wunch, D., and Yoshimizu, J.:
1749 The Orbiting Carbon Observatory-2: first 18 months of science data products, *Atmos. Meas.*
1750 *Tech.*, 10, 549–563, <https://doi.org/10.5194/amt-10-549-2017>, 2017.

1751 Eldering, A., Taylor, T. E., O'Dell, C. W., and Pavlick, R.: The OCO-3 mission:
1752 measurement objectives and expected performance based on 1 year of simulated data, *Atmos.*
1753 *Meas. Tech.*, 12, 2341–2370, <https://doi.org/10.5194/amt-12-2341-2019>, 2019.

1754 Fan, N., & Forkel, M. (2025). Drivers of the enhanced amplitude of atmospheric CO₂ in
1755 northern terrestrial ecosystems. <https://doi.org/10.5194/egusphere-egu25-7279>

1756 Fang, S. X., Tans, P. P., Steinbacher, M., Zhou, L. X., and Luan, T.: Comparison of the
1757 regional CO₂ mole fraction filtering approaches at a WMO/GAW regional station in China,
1758 *Atmospheric Measurement Techniques*, 8, 5301–5313, [https://doi.org/10.5194/amt-8-5301-](https://doi.org/10.5194/amt-8-5301-2015)
1759 [2015](https://doi.org/10.5194/amt-8-5301-2015), 2015.

1760 Fawzy, S., Osman, A. I., Doran, J., and Rooney, D. W.: Strategies for mitigation of climate
1761 change: a review, *Environ Chem Lett*, 18, 2069–2094, [https://doi.org/10.1007/s10311-020-](https://doi.org/10.1007/s10311-020-01059-w)
1762 [01059-w](https://doi.org/10.1007/s10311-020-01059-w), 2020.

1763 Frankenberg, C., O'Dell, C., Berry, J., Guanter, L., Joiner, J., Köhler, P., Pollock, R., and
1764 Taylor, T. E.: Prospects for chlorophyll fluorescence remote sensing from the Orbiting
1765 Carbon Observatory-2, *Remote Sensing of Environment*, 147, 1–12,
1766 <https://doi.org/10.1016/j.rse.2014.02.007>, 2014.

1767 Friedlingstein, P., O'Sullivan, M., Jones, M. W., Andrew, R. M., Hauck, J., Landschützer, P.,
1768 Le Quééré, C., Li, H., Luijckx, I. T., Olsen, A., Peters, G. P., Peters, W., Pongratz, J.,
1769 Schwingshackl, C., Sitch, S., Canadell, J. G., Ciais, P., Jackson, R. B., Alin, S. R., Arneeth, A.,
1770 Arora, V., Bates, N. R., Becker, M., Bellouin, N., Berghoff, C. F., Bittig, H. C., Bopp, L.,
1771 Cadule, P., Campbell, K., Chamberlain, M. A., Chandra, N., Chevallier, F., Chini, L. P.,
1772 Colligan, T., Decayeux, J., Djeutchouang, L. M., Dou, X., Duran Rojas, C., Enyo, K., Evans,
1773 W., Fay, A. R., Feely, R. A., Ford, D. J., Foster, A., Gasser, T., Gehlen, M., Gkritzalis, T.,
1774 Grassi, G., Gregor, L., Gruber, N., Gürses, Ö., Harris, I., Hefner, M., Heinke, J., Hurtt, G. C.,
1775 Iida, Y., Ilyina, T., Jacobson, A. R., Jain, A. K., Jarníková, T., Jersild, A., Jiang, F., Jin, Z.,
1776 Kato, E., Keeling, R. F., Klein Goldewijk, K., Knauer, J., Korsbakken, J. I., Lan, X., Lauvset,
1777 S. K., Lefèvre, N., Liu, Z., Liu, J., Ma, L., Maksyutov, S., Marland, G., Mayot, N., McGuire,
1778 P. C., Metzl, N., Monacci, N. M., Morgan, E. J., Nakaoka, S.-I., Neill, C., Niwa, Y., Nützel,
1779 T., Olivier, L., Ono, T., Palmer, P. I., Pierrot, D., Qin, Z., Resplandy, L., Roobaert, A.,
1780 Rosan, T. M., Rödenbeck, C., Schwinger, J., Smallman, T. L., Smith, S. M., Sospedra-
1781 Alfonso, R., Steinhoff, T., et al.: Global Carbon Budget 2024, *Earth Syst. Sci. Data*, 17, 965–
1782 [1039](https://doi.org/10.5194/essd-17-965-2025), <https://doi.org/10.5194/essd-17-965-2025>, 2025.

1783 Halder, S., Tiwari, Y. K., Valsala, V., Sreeush, M. G., Sijikumar, S., Janardanan, R., &
1784 Maksyutov, S. (2021). Quantification of enhancement in atmospheric CO₂ background due to
1785 Indian biospheric fluxes and fossil fuel emissions. *Journal of Geophysical Research:*
1786 *Atmospheres*, 126(13), e2021JD034545.

1787 Harriss, R. C., Sachse, G. W., Collins Jr., J. E., Wade, L., Bartlett, K. B., Talbot, R. W.,
1788 Browell, E. V., Barrie, L. A., Hill, G. F., and Burney, L. G.: Carbon monoxide and methane

1789 [over Canada: July–August 1990, Journal of Geophysical Research: Atmospheres, 99, 1659–](#)
1790 [1669, https://doi.org/10.1029/93JD01906, 1994.](#)

1791 [Huang, J., Golombek, A., Prinn, R., Weiss, R., Fraser, P., Simmonds, P., Dlugokencky, E. J.,](#)
1792 [Hall, B., Elkins, J., Steele, P., Langenfelds, R., Krummel, P., Dutton, G., and Porter, L.:](#)
1793 [Estimation of regional emissions of nitrous oxide from 1997 to 2005 using multinetwork](#)
1794 [measurements, a chemical transport model, and an inverse method, Journal of Geophysical](#)
1795 [Research: Atmospheres, 113, https://doi.org/10.1029/2007JD009381, 2008.](#)

1796 [Huang, J., Yu, H., Guan, X., Wang, G., and Guo, R.: Accelerated dryland expansion under](#)
1797 [climate change, Nature Clim Change, 6, 166–171, https://doi.org/10.1038/nclimate2837,](#)
1798 [2016.](#)

1799 [IPCC, 2021: Climate Change 2021: The Physical Science Basis. Contribution of Working](#)
1800 [Group I to the Sixth Assessment Report of the Intergovernmental Panel on Climate](#)
1801 [Change\[Masson-Delmotte, V., P. Zhai, A. Pirani, S.L. Connors, C. Péan, S. Berger, N. Caud,](#)
1802 [Y. Chen, L. Goldfarb, M.I. Gomis, M. Huang, K. Leitzell, E. Lonnoy, J.B.R. Matthews, T.K.](#)
1803 [Maycock, T. Waterfield, O. Yelekçi, R. Yu, and B. Zhou \(eds.\)\]. Cambridge University](#)
1804 [Press, Cambridge, United Kingdom and New York, NY, USA, In press,](#)
1805 [doi:10.1017/9781009157896.](#)

1806 [Ito, A.: Disequilibrium of terrestrial ecosystem CO₂ budget caused by disturbance-induced](#)
1807 [emissions and non-CO₂ carbon export flows: a global model assessment, Earth Syst. Dynam.,](#)
1808 [10, 685–709, https://doi.org/10.5194/esd-10-685-2019, 2019.](#)

1809 [Jain, C. D., Singh, V., Akhil Raj, S. T., Madhavan, B. L., and Ratnam, M. V.: Local emission](#)
1810 [and long-range transport impacts on the CO, CO₂, and CH₄ concentrations at a tropical rural](#)
1811 [site, Atmospheric Environment, 254, 118397,](#)
1812 [https://doi.org/10.1016/j.atmosenv.2021.118397, 2021.](#)

1813 [Jing, X., Huang, J., Wang, G., Higuchi, K., Bi, J., Sun, Y., Yu, H., and Wang, T.: The effects](#)
1814 [of clouds and aerosols on net ecosystem CO₂ exchange over semi-arid Loess Plateau of](#)
1815 [Northwest China, Atmospheric Chemistry and Physics, 10, 8205–8218,](#)
1816 [https://doi.org/10.5194/acp-10-8205-2010, 2010.](#)

1817 [Joiner, J. and Yoshida, Y.: Satellite-based reflectances capture large fraction of variability in](#)
1818 [global gross primary production \(GPP\) at weekly time scales, Agricultural and Forest](#)
1819 [Meteorology, 291, 108092, https://doi.org/10.1016/j.agrformet.2020.108092, 2020.](#)

1820 [Joiner, J., Yoshida, Y., Zhang, Y., Duveiller, G., Jung, M., Lyapustin, A., Wang, Y., and](#)
1821 [Tucker, C. J.: Estimation of Terrestrial Global Gross Primary Production \(GPP\) with Satellite](#)
1822 [Data-Driven Models and Eddy Covariance Flux Data, Remote Sensing, 10, 1346,](#)
1823 [https://doi.org/10.3390/rs10091346, 2018.](#)

1824 [Jones, M. W., Andrew, R. M., Peters, G. P., Janssens-Maenhout, G., De-Gol, A. J., Ciais, P.,](#)
1825 [Patra, P. K., Chevallier, F., and Le Quéré, C.: Gridded fossil CO₂ emissions and related O₂](#)
1826 [combustion consistent with national inventories 1959–2018, Sci Data, 8, 2,](#)
1827 [https://doi.org/10.1038/s41597-020-00779-6, 2021.](#)

1828 [Kar, J., Bremer, H., Drummond, J. R., Rochon, Y. J., Jones, D. B. A., Nichitiu, F., Zou, J.,](#)
1829 [Liu, J., Gille, J. C., Edwards, D. P., Deeter, M. N., Francis, G., Ziskin, D., and Warner, J.:](#)

1830 [Evidence of vertical transport of carbon monoxide from Measurements of Pollution in the](#)
1831 [Troposphere \(MOPITT\), Geophysical Research Letters, 31,](#)
1832 <https://doi.org/10.1029/2004GL021128>, 2004.

1833 [Krishnapriya, M., Pattanaik, D. R., Kumar, A., Ramana, M. V., & Naidu, C. V. \(2025\).](#)
1834 [Spatio-temporal dynamics of atmospheric CO₂ over India and its inter-relationship with](#)
1835 [combustion emissions, ecosystem exchange, and meteorological factors: M Krishnapriya et](#)
1836 [al. *Journal of Earth System Science*, 134\(4\), 193.](#)

1837 [Krol, M., Houweling, S., Bregman, B., van den Broek, M., Segers, A., van Velthoven, P.,](#)
1838 [Peters, W., Dentener, F., and Bergamaschi, P.: The two-way nested global chemistry-](#)
1839 [transport zoom model TM5: algorithm and applications, *Atmospheric Chemistry and Physics*](#)
1840 [Discussions, 4, 3975–4018, 2004.](#)

1841 [Kumar, A., Yu, Z.-G., Klemeš, J. J., and Bokhari, A.: A state-of-the-art review of greenhouse](#)
1842 [gas emissions from Indian hydropower reservoirs, *Journal of Cleaner Production*, 320,](#)
1843 [128806, https://doi.org/10.1016/j.jclepro.2021.128806](https://doi.org/10.1016/j.jclepro.2021.128806), 2021.

1844 [Kunchala, R. K., Girach, I., Das, C., Jain, C., Burman, P. K. D., Pathakoti, M., ... & Jain, V.](#)
1845 [\(2025\). Carbon dioxide \(CO₂\) variations across India: Synthesis of observations and model](#)
1846 [simulations. *Atmospheric Environment*, 121746.](#)

1847 [Kunchala, R. K., Patra, P. K., Kumar, K. N., Chandra, N., Attada, R., and Karumuri, R. K.:](#)
1848 [Spatio-temporal variability of XCO₂ over Indian region inferred from Orbiting Carbon](#)
1849 [Observatory \(OCO-2\) satellite and Chemistry Transport Model, *Atmospheric Research*, 269,](#)
1850 [106044, https://doi.org/10.1016/j.atmosres.2022.106044](https://doi.org/10.1016/j.atmosres.2022.106044), 2022.

1851 [Kuttiappurath, J., Peter, R., Singh, A., and Raj, S.: The increasing atmospheric CO₂ over](#)
1852 [India: Comparison to global trends, *iScience*, 25, 104863,](#)
1853 <https://doi.org/10.1016/j.isci.2022.104863>, 2022.

1854 [Lai, S. C., Baker, A. K., Schuck, T. J., van Velthoven, P., Oram, D. E., Zahn, A., Hermann,](#)
1855 [M., Weigelt, A., Slemr, F., Brenninkmeijer, C. a. M., and Ziereis, H.: Pollution events](#)
1856 [observed during CARIBIC flights in the upper troposphere between South China and the](#)
1857 [Philippines, *Atmospheric Chemistry and Physics*, 10, 1649–1660,](#)
1858 <https://doi.org/10.5194/acp-10-1649-2010>, 2010.

1859 [Le Quéré, C., Andrew, R. M., Friedlingstein, P., Sitch, S., Pongratz, J., Manning, A. C.,](#)
1860 [Korsbakken, J. I., Peters, G. P., Canadell, J. G., Jackson, R. B., Boden, T. A., Tans, P. P.,](#)
1861 [Andrews, O. D., Arora, V. K., Bakker, D. C. E., Barbero, L., Becker, M., Betts, R. A., Bopp,](#)
1862 [L., Chevallier, F., Chini, L. P., Ciais, P., Cosca, C. E., Cross, J., Currie, K., Gasser, T., Harris,](#)
1863 [I., Hauck, J., Haverd, V., Houghton, R. A., Hunt, C. W., Hurtt, G., Ilyina, T., Jain, A. K.,](#)
1864 [Kato, E., Kautz, M., Keeling, R. F., Klein Goldewijk, K., Körtzinger, A., Landschützer, P.,](#)
1865 [Lefèvre, N., Lenton, A., Lienert, S., Lima, I., Lombardozzi, D., Metzl, N., Millero, F.,](#)
1866 [Monteiro, P. M. S., Munro, D. R., Nabel, J. E. M. S., Nakaoka, S., Nojiri, Y., Padin, X. A.,](#)
1867 [Peregon, A., Pfeil, B., Pierrot, D., Poulter, B., Rehder, G., Reimer, J., Rödenbeck, C.,](#)
1868 [Schwinger, J., Séférian, R., Skjelvan, I., Stocker, B. D., Tian, H., Tilbrook, B., Tubiello, F.](#)
1869 [N., Van Der Laan-Luijkx, I. T., Van Der Werf, G. R., Van Heuven, S., Viovy, N., Vuichard,](#)
1870 [N., Walker, A. P., Watson, A. J., Wiltshire, A. J., Zaehle, S., and Zhu, D.: Global Carbon](#)
1871 [Budget 2017, *Earth Syst. Sci. Data*, 10, 405–448, https://doi.org/10.5194/essd-10-405-2018,](#)
1872 [2018.](#)

1873 [Laurent, O., 2016. ICOS Atmospheric Station Specifications.](#)

1874

1875 [Lin, X., Indira, N. K., Ramonet, M., Delmotte, M., Ciais, P., Bhatt, B. C., Reddy, M. V.,](#)

1876 [Angchuk, D., Balakrishnan, S., Jorphail, S., Dorjai, T., Mahey, T. T., Patnaik, S., Begum, M.,](#)

1877 [Brenninkmeijer, C., Durairaj, S., Kirubakaran, R., Schmidt, M., Swathi, P. S., Vinithkumar,](#)

1878 [N. V., Yver Kwok, C., and Gaur, V. K.: Long-lived atmospheric trace gases measurements in](#)

1879 [flask samples from three stations in India, Atmos. Chem. Phys., 15, 9819–9849,](#)

1880 <https://doi.org/10.5194/acp-15-9819-2015>, 2015.

1881 [Lin, X., Ciais, P., Bousquet, P., Ramonet, M., Yin, Y., Balkanski, Y., Cozic, A., Delmotte,](#)

1882 [M., Evangeliou, N., Indira, N. K., Locatelli, R., Peng, S., Piao, S., Saunio, M., Swathi, P. S.,](#)

1883 [Wang, R., Yver-Kwok, C., Tiwari, Y. K., and Zhou, L.: Simulating CH₄ and CO₂ over South](#)

1884 [and East Asia using the zoomed chemistry transport model LMDz-INCA, Atmos. Chem.](#)

1885 [Phys., 18, 9475–9497, https://doi.org/10.5194/acp-18-9475-2018](#), 2018.

1886 [Liu, J., Bowman, K. W., Lee, M., Henze, D. K., Bousseres, N., Brix, H., Collatz, G. J.,](#)

1887 [Menemenlis, D., Ott, L., Pawson, S., Jones, D., and Nassar, R.: Carbon monitoring system](#)

1888 [flux estimation and attribution: impact of ACOS-GOSAT XCO₂ sampling on the inference of](#)

1889 [terrestrial biospheric sources and sinks, Tellus B: Chemical and Physical Meteorology, 66,](#)

1890 [22486, https://doi.org/10.3402/tellusb.v66.22486](https://doi.org/10.3402/tellusb.v66.22486), 2014.

1891 [Lopez, M.: Estimation des émissions de gaz à effet de serre à différentes échelles en France à](#)

1892 [l'aide d'observations de haute précision, phdthesis, Université Paris Sud - Paris XI, 2012.](#)

1893 [Mahesh, P., Sreenivas, G., Rao, P. V. N., Dadhwal, V. K., Sai Krishna, S. V. S., and](#)

1894 [Mallikarjun, K.: High-precision surface-level CO₂ and CH₄ using off-axis integrated cavity](#)

1895 [output spectroscopy \(OA-ICOS\) over Shadnagar, India, International Journal of Remote](#)

1896 [Sensing, 36, 5754–5765, https://doi.org/10.1080/01431161.2015.1104744](#), 2015.

1897 [Masarie, K. A., Peters, W., Jacobson, A. R., and Tans, P. P.: ObsPack: a framework for the](#)

1898 [preparation, delivery, and attribution of atmospheric greenhouse gas measurements, Earth](#)

1899 [Syst. Sci. Data, 6, 375–384, https://doi.org/10.5194/essd-6-375-2014](#), 2014.

1900 [Matsueda, H., Inoue, H. Y., Ishii, M., and Tsutsumi, Y.: Large injection of carbon monoxide](#)

1901 [into the upper troposphere due to intense biomass burning in 1997, J. Geophys. Res., 104,](#)

1902 [26867–26879, https://doi.org/10.1029/1999JD900193](https://doi.org/10.1029/1999JD900193), 1999.

1903 [Mauzerall, D. L., Logan, J. A., Jacob, D. J., Anderson, B. E., Blake, D. R., Bradshaw, J. D.,](#)

1904 [Heikes, B., Sachse, G. W., Singh, H., and Talbot, B.: Photochemistry in biomass burning](#)

1905 [plumes and implications for tropospheric ozone over the tropical South Atlantic, J. Geophys.](#)

1906 [Res., 103, 8401–8423, https://doi.org/10.1029/97JD02612](#), 1998.

1907 [Metya, A., Datye, A., Chakraborty, S., Tiwari, Y. K., Sarma, D., Bora, A., and Gogoi, N.:](#)

1908 [Diurnal and seasonal variability of CO₂ and CH₄ concentration in a semi-urban environment](#)

1909 [of western India, Sci Rep, 11, 2931, https://doi.org/10.1038/s41598-021-82321-1](#), 2021.

1910 [Mühle, J., Brenninkmeijer, C. a. M., Rhee, T. S., Slemr, F., Oram, D. E., Penkett, S. A., and](#)

1911 [Zahn, A.: Biomass burning and fossil fuel signatures in the upper troposphere observed](#)

1912 [during a CARIBIC flight from Namibia to Germany, Geophysical Research Letters, 29, 16-1-](#)

1913 [16–4, https://doi.org/10.1029/2002GL015764](https://doi.org/10.1029/2002GL015764), 2002.

1914 [Munksgaard, N. C., Lee, I. L., Napier, T. P., Zwart, C., Cernusak, L. A., & Bird, M. I. \(2022\).
1915 One year of spectroscopic high-frequency measurements of atmospheric CO₂, CH₄, H.
1916 Geoscience Data Journal. <https://doi.org/10.1002/gdj3.180>](#)

1917 [Nalini, K., Sijikumar, S., Valsala, V., Tiwari, Y. K., and Ramachandran, R.: Designing
1918 surface CO₂ monitoring network to constrain the Indian land fluxes. Atmospheric
1919 Environment, 218, 117003, <https://doi.org/10.1016/j.atmosenv.2019.117003>, 2019.](#)

1920 [Nath, B.: Quantitative Assessment of Forest Cover Change of a Part of Bandarban Hill Tracts
1921 Using NDVI Techniques, Journal of Geosciences and Geomatics, 2, 21–27,
1922 <https://doi.org/10.12691/jgg-2-1-4>, 2014.](#)

1923 [Nishanth, T., Praseed, K. M., Kumar, M. K. S., and Valsaraj, K. T.: Observational Study of
1924 Surface O₃, NO_x, CH₄ and Total NMHCs at Kannur, India, Aerosol Air Qual. Res., 14,
1925 1074–1088, <https://doi.org/10.4209/aaqr.2012.11.0323>, 2014.](#)

1926 [Niwa, Y., Machida, T., Sawa, Y., Matsueda, H., Schuck, T. J., Brenninkmeijer, C. A. M.,
1927 Imasu, R., and Satoh, M.: Imposing strong constraints on tropical terrestrial CO₂ fluxes using
1928 passenger aircraft based measurements, Journal of Geophysical Research: Atmospheres, 117,
1929 <https://doi.org/10.1029/2012JD017474>, 2012.](#)

1930 [Nomura, S., Naja, M., Ahmed, M. K., Mukai, H., Terao, Y., Machida, T., Sasakawa, M., and
1931 Patra, P. K.: Measurement report: Regional characteristics of seasonal and long-term
1932 variations in greenhouse gases at Nainital, India, and Comilla, Bangladesh, Atmos. Chem.
1933 Phys., 21, 16427–16452, <https://doi.org/10.5194/acp-21-16427-2021>, 2021.](#)

1934 [Paris, J.-D., Ciais, P., Nédélec, P., Ramonet, M., Belan, B. D., Arshinov, M. Yu., Golitsyn, G.
1935 S., Granberg, I., Stohl, A., Cayez, G., Athier, G., Boumard, F., and Cousin, J.-M.: The YAK-
1936 AEROSIB transcontinental aircraft campaigns: new insights on the transport of CO₂, CO and
1937 O₃ across Siberia, Tellus B: Chemical and Physical Meteorology, 60, 551–568,
1938 <https://doi.org/10.1111/j.1600-0889.2008.00369.x>, 2008.](#)

1939 [Park, M., Randel, W. J., Emmons, L. K., and Livesey, N. J.: Transport pathways of carbon
1940 monoxide in the Asian summer monsoon diagnosed from Model of Ozone and Related
1941 Tracers \(MOZART\), J. Geophys. Res., 114, 2008JD010621,
1942 <https://doi.org/10.1029/2008JD010621>, 2009.](#)

1943 [Pathakoti, M., D.V., M., Gaddamidi, S., Arun, S. S., Bothale, R. V., Chauhan, P., P. R., K.S.,
1944 R., and Chandra, N.: Three-dimensional view of CO₂ variability in the atmosphere over the
1945 Indian region, Atmospheric Research, 290, 106785,
1946 <https://doi.org/10.1016/j.atmosres.2023.106785>, 2023.](#)

1947 [Patil, M. N., Dharmaraj, T., Waghmare, R. T., Prabha, T. V., and Kulkarni, J. R.:
1948 Measurements of carbon dioxide and heat fluxes during monsoon-2011 season over rural site
1949 of India by eddy covariance technique, J Earth Syst Sci, 123, 177–185,
1950 <https://doi.org/10.1007/s12040-013-0374-z>, 2014.](#)

1951 [Patra, P. K., Niwa, Y., Schuck, T. J., Brenninkmeijer, C. a. M., Machida, T., Matsueda, H.,
1952 and Sawa, Y.: Carbon balance of South Asia constrained by passenger aircraft CO₂
1953 measurements, Atmospheric Chemistry and Physics, 11, 4163–4175,
1954 <https://doi.org/10.5194/acp-11-4163-2011>, 2011.](#)

1955 [Patra, P. K., Canadell, J. G., Houghton, R. A., Piao, S. L., Oh, N.-H., Ciais, P., Manjunath, K.](#)
1956 [R., Chhabra, A., Wang, T., Bhattacharya, T., Bousquet, P., Hartman, J., Ito, A., Mayorga, E.,](#)
1957 [Niwa, Y., Raymond, P. A., Sarma, V. V. S. S., and Lasco, R.: The carbon budget of South](#)
1958 [Asia, *Biogeosciences*, 10, 513–527, <https://doi.org/10.5194/bg-10-513-2013>, 2013.](#)

1959 [Patra, P. K., Crisp, D., Kaiser, J. W., Wunch, D., Saeki, T., Ichii, K., Sekiya, T., Wennberg,](#)
1960 [P. O., Feist, D. G., Pollard, D. F., Griffith, D. W. T., Velazco, V. A., De Maziere, M., Sha, M.](#)
1961 [K., Roehl, C., Chatterjee, A., and Ishijima, K.: The Orbiting Carbon Observatory \(OCO-2\)](#)
1962 [tracks 2–3 peta-gram increase in carbon release to the atmosphere during the 2014–2016 El](#)
1963 [Niño, *Sci Rep.* 7, 13567, <https://doi.org/10.1038/s41598-017-13459-0>, 2017.](#)

1964 [Patra, P. K., Takigawa, M., Watanabe, S., Chandra, N., Ishijima, K., and Yamashita, Y.:](#)
1965 [Improved Chemical Tracer Simulation by MIROC4.0-based Atmospheric Chemistry-](#)
1966 [Transport Model \(MIROC4-ACTM\), *Sola*, 14, 91–96, <https://doi.org/10.2151/sola.2018-016>,](#)
1967 [2018.](#)

1968 [Peters, W., Miller, J. B., Whitaker, J., Denning, A. S., Hirsch, A., Krol, M. C., Zupanski, D.,](#)
1969 [Bruhwiler, L., and Tans, P. P.: An ensemble data assimilation system to estimate CO₂ surface](#)
1970 [fluxes from atmospheric trace gas observations, *Journal of Geophysical Research:*](#)
1971 [Atmospheres, 110, <https://doi.org/10.1029/2005JD006157>, 2005.](#)

1972 [Philip, S., Johnson, M. S., Potter, C., Genovesse, V., Baker, D. F., Haynes, K. D., Henze, D.](#)
1973 [K., Liu, J., and Poulter, B.: Prior biosphere model impact on global terrestrial CO₂ fluxes](#)
1974 [estimated from OCO-2 retrievals, *Atmos. Chem. Phys.*, 19, 13267–13287,](#)
1975 [<https://doi.org/10.5194/acp-19-13267-2019>, 2019.](#)

1976 [Philip, S., Johnson, M. S., Baker, D. F., Basu, S., Tiwari, Y. K., Indira, N. K., Ramonet, M.,](#)
1977 [and Poulter, B.: OCO-2 Satellite-Imposed Constraints on Terrestrial Biospheric CO₂ Fluxes](#)
1978 [Over South Asia, *JGR Atmospheres*, 127, e2021JD035035,](#)
1979 [<https://doi.org/10.1029/2021JD035035>, 2022.](#)

1980 [Potter, C. S., Randerson, J. T., Field, C. B., Matson, P. A., Vitousek, P. M., Mooney, H. A.,](#)
1981 [and Klooster, S. A.: Terrestrial ecosystem production: A process model based on global](#)
1982 [satellite and surface data, *Global Biogeochemical Cycles*, 7, 811–841,](#)
1983 [<https://doi.org/10.1029/93GB02725>, 1993.](#)

1984 [Randel, W. J. and Park, M.: Deep convective influence on the Asian summer monsoon](#)
1985 [anticyclone and associated tracer variability observed with Atmospheric Infrared Sounder](#)
1986 [\(AIRS\), *Journal of Geophysical Research: Atmospheres*, 111,](#)
1987 [<https://doi.org/10.1029/2005JD006490>, 2006.](#)

1988 [Randerson, J. T., Thompson, M. V., Conway, T. J., Fung, I. Y., and Field, C. B.: The](#)
1989 [contribution of terrestrial sources and sinks to trends in the seasonal cycle of atmospheric](#)
1990 [carbon dioxide, *Global Biogeochemical Cycles*, 11, 535–560,](#)
1991 [<https://doi.org/10.1029/97GB02268>, 1997.](#)

1992 [Rathore, J., Ganguly, D., Singh, V., Gupta, M., Vazhathara, V. J., Biswal, A., Kunchala, R.](#)
1993 [K., Patra, P. K., Sahu, L. K., Gani, S., and Dey, S.: Characteristics of Haze Pollution Events](#)
1994 [During Biomass Burning Period at an Upwind Site of Delhi, *JGR Atmospheres*, 130,](#)
1995 [e2024JD042347, <https://doi.org/10.1029/2024JD042347>, 2025.](#)

1996 [Rayner, P. J., Law, R. M., Allison, C. E., Francey, R. J., Trudinger, C. M., and Pickett-Heaps, C.:](#) Interannual variability of the global carbon cycle (1992–2005) inferred by inversion of atmospheric CO₂ and δ¹³C_{CO₂} measurements, *Global Biogeochemical Cycles*, 22, <https://doi.org/10.1029/2007GB003068>, 2008.

1997

1998

1999

2000 [Reid, K. H. and Steyn, D. G.:](#) Diurnal variations of boundary-layer carbon dioxide in a coastal city—Observations and comparison with model results, *Atmospheric Environment*, 31, 3101–3114, [https://doi.org/10.1016/S1352-2310\(97\)00050-2](https://doi.org/10.1016/S1352-2310(97)00050-2), 1997.

2001

2002

2003 [Russo, R. S., Talbot, R. W., Dibb, J. E., Scheuer, E., Seid, G., Jordan, C. E., Fuelberg, H. E., Sachse, G. W., Avery, M. A., Vay, S. A., Blake, D. R., Blake, N. J., Atlas, E., Fried, A., Sandholm, S. T., Tan, D., Singh, H. B., Snow, J., and Heikes, B. G.:](#) Chemical composition of Asian continental outflow over the western Pacific: Results from Transport and Chemical Evolution over the Pacific (TRACE-P), *Journal of Geophysical Research: Atmospheres*, 108, <https://doi.org/10.1029/2002JD003184>, 2003.

2004

2005

2006

2007 [Sawa, Y., Matsueda, H., Makino, Y., Inoue, H. Y., Murayama, S., Hirota, M., Tsutsumi, Y., Zaizen, Y., Ikegami, M., and Okada, K.:](#) Aircraft Observation of CO₂, CO₂ O₃ and H₂ over the North Pacific during the PACE-7 Campaign, *Tellus B: Chemical and Physical Meteorology*, 56, 2, <https://doi.org/10.3402/tellusb.v56i1.16402>, 2004.

2008

2009

2010

2011

2012 [Schaaf, C. and Wang, Z.:](#) MODIS/Terra+Aqua BRDF/Albedo Nadir BRDF-Adjusted Ref Band6 Daily L3 Global 30ArcSec CMG V061, <https://doi.org/10.5067/MODIS/MCD43D67.061>, 2021.

2013

2014

2015

2016 [Schaaf, C. B., Gao, F., Strahler, A. H., Lucht, W., Li, X., Tsang, T., Strugnell, N. C., Zhang, X., Jin, Y., Muller, J.-P., Lewis, P., Barnsley, M., Hobson, P., Disney, M., Roberts, G., Dunderdale, M., Doll, C., d'Entremont, R. P., Hu, B., Liang, S., Privette, J. L., and Roy, D.:](#) First operational BRDF, albedo nadir reflectance products from MODIS, *Remote Sensing of Environment*, 83, 135–148, [https://doi.org/10.1016/S0034-4257\(02\)00091-3](https://doi.org/10.1016/S0034-4257(02)00091-3), 2002.

2017

2018

2019

2020

2021 [Schuck, T. J., Ishijima, K., Patra, P. K., Baker, A. K., Machida, T., Matsueda, H., Sawa, Y., Umezawa, T., Brenninkmeijer, C. a. M., and Lelieveld, J.:](#) Distribution of methane in the tropical upper troposphere measured by CARIBIC and CONTRAIL aircraft, *Journal of Geophysical Research: Atmospheres*, 117, <https://doi.org/10.1029/2012JD018199>, 2012.

2022

2023

2024

2025 [Schuldt, K. N., Mund, J., Aalto, T., Abshire, J. B., Aikin, K., Allen, G., Andrade, M., Arlyn Andrews, Apadula, F., Arnold, S., Baier, B., Bakwin, P., Bäni, L., Bartyzel, J., Bentz, G., Bergamaschi, P., Beyersdorf, A., Biermann, T., Biraud, S. C., Pierre-Eric Blanc, Boenisch, H., Bowling, D., Brailsford, G., Brand, W. A., Brunner, D., Bui, T. P. V., Van Den Bulk, P., Benoit Burban, Francescopiero Calzolari, Chang, C. S., Chen, G., Huilin Chen, Lukasz Chmura, St. Clair, J. M., Clark, S., Sites Climadat, Coletta, J. D., Colomb, A., Commane, R., Condori, L., Conen, F., Conil, S., Couret, C., Cristofanelli, P., Cuevas, E., Curcoll, R., Daube, B., Davis, K. J., Dean-Day, J. M., Delmotte, M., Dickerson, R., DiGangi, E., DiGangi, J. P., Van Dinter, D., Elsasser, M., Emmenegger, L., Shuangxi Fang, Forster, G., France, J., Frumau, A., Fuente-Lastra, M., Galkowski, M., Gatti, L. V., Gehrlein, T., Gerbig, C., Francois Gheusi, Gloor, E., Goto, D., Griffis, T., Hammer, S., Hanisco, T. F., Hanson, C., Haszpra, L., Hatakka, J., Heimann, M., Heliasz, M., Heltai, D., Henne, S., Hensen, A., Hermans, C., Hermansen, O., Hintsa, E., Hoheisel, A., Holst, J., Di Iorio, T., Iraci, L. T., Ivakhov, V., Jaffe, D. A., Jordan, A., Joubert, W., Kang, H.-Y., Karion, A., Kawa, S. R., Kazan, V., Keeling, R. F., Keronen, P., Jooil Kim, Klausen, J., Kneuer, T., et al.:](#) Multi-

2040 [laboratory compilation of atmospheric carbon dioxide data for the period 1957-2023;](#)
2041 [obspack_co2_1_GLOBALVIEWplus_v10.1_2024-11-13,](#)
2042 [https://doi.org/10.25925/20241101.2024.](https://doi.org/10.25925/20241101.2024)

2043 [Sharma, N., Dadhwal, V. K., Kant, Y., Mahesh, P., Mallikarjun, K., Gadavi, H., Sharma, A.,](#)
2044 [and Ali, M. M.: Atmospheric CO₂ Variations in Two Contrasting Environmental Sites Over](#)
2045 [India, Air, Soil and Water Research, 7, ASWR.S13987,](#)
2046 <https://doi.org/10.4137/ASWR.S13987>, 2014.

2047 [Sreenivas, G., Mahesh, P., Subin, J., Kanchana, A. L., Rao, P. V. N., and Dadhwal, V. K.:](#)
2048 [Influence of Meteorology and interrelationship with greenhouse gases](#)
2049 [\(CO₂ and CH₄\) at a suburban site of India,](#)
2050 [Atmos. Chem. Phys., 16, 3953–3967, https://doi.org/10.5194/acp-16-3953-2016, 2016.](#)

2051 [Sreenivas, G., P., M., Mahalakshmi, D. V., Kanchana, A. L., Chandra, N., Patra, P. K., Raja,](#)
2052 [P., Sessa Sai, M. V. R., Sripada, S., Rao, P. V. N., and Dadhwal, V. K.: Seasonal and annual](#)
2053 [variations of CO₂ and CH₄ at Shadnagar, a semi-urban site, Science of The Total](#)
2054 [Environment, 819, 153114, https://doi.org/10.1016/j.scitotenv.2022.153114, 2022.](#)

2055 [Srivastava, P., Bennett, M. W., Bedrosian, G., Rosenberg, R., Solish, B., and Basilio, R. R.:](#)
2056 [Establishing Launch Readiness of NASA ISS Instrument OCO-3, in: IGARSS 2020 - 2020](#)
2057 [IEEE International Geoscience and Remote Sensing Symposium, IGARSS 2020 - 2020 IEEE](#)
2058 [International Geoscience and Remote Sensing Symposium, Waikoloa, HI, USA, 6101–6104,](#)
2059 <https://doi.org/10.1109/IGARSS39084.2020.9323631>, 2020.

2060 [Stocker, T.F., D. Qin, G.-K. Plattner, L.V. Alexander, S.K. Allen, N.L. Bindoff, F.-M. Bréon,](#)
2061 [J.A. Church, U. Cubasch, S. Emori, P. Forster, P. Friedlingstein, N. Gillett, J.M. Gregory,](#)
2062 [D.L. Hartmann, E. Jansen, B. Kirtman, R. Knutti, K. Krishna Kumar, P. Lemke, J. Marotzke,](#)
2063 [V.Masson-Delmotte, G.A. Meehl, I.I. Mokhov, S. Piao, V. Ramaswamy, D. Randall, M.](#)
2064 [Rhein, M. Rojas, C. Sabine, D. Shindell, L.D. Talley, D.G. Vaughan and S.-P. Xie, 2013:](#)
2065 [Technical Summary. In: Climate Change 2013: The Physical Science Basis. Contribution of](#)
2066 [Working Group I to the Fifth Assessment Report of the Intergovernmental Panel on Climate](#)
2067 [Change \[Stocker, T.F., D. Qin, G.-K. Plattner, M. Tignor, S.K. Allen, J. Boschung, A.](#)
2068 [Nauels, Y. Xia, V. Bex and P.M. Midgley \(eds.\)\]. Cambridge University Press, Cambridge,](#)
2069 [United Kingdom and New York, NY, USA](#)

2070 [Stull, R. B. \(Ed.\): An Introduction to Boundary Layer Meteorology, Springer Netherlands,](#)
2071 [Dordrecht, https://doi.org/10.1007/978-94-009-3027-8, 1988.](#)

2072 [Summa, D., Di Girolamo, P., Stelitano, D., and Cacciani, M.: Characterization of the](#)
2073 [planetary boundary layer height and structure by Raman lidar: comparison of different](#)
2074 [approaches, Atmospheric Measurement Techniques, 6, 3515–3525,](#)
2075 <https://doi.org/10.5194/amt-6-3515-2013>, 2013.

2076 [Sun, Y., Frankenberg, C., Jung, M., Joiner, J., Guanter, L., Köhler, P., and Magney, T.:](#)
2077 [Overview of Solar-Induced chlorophyll Fluorescence \(SIF\) from the Orbiting Carbon](#)
2078 [Observatory-2: Retrieval, cross-mission comparison, and global monitoring for GPP, Remote](#)
2079 [Sensing of Environment, 209, 808–823, https://doi.org/10.1016/j.rse.2018.02.016, 2018.](#)

2080 [Thilakan, V., Pillai, D., Sukumaran, J., Gerbig, C., Hakkim, H., Sinha, V., Terao, Y., Naja,](#)
2081 [M., and Deshpande, M. V.: Potential of using CO₂ observations over India in regional carbon](#)

2082 [budget estimation by improving the modelling system, EGU sphere, 1–32,](#)
2083 <https://doi.org/10.5194/egusphere-2023-1582>, 2023.

2084 [Tiwari, Y., Valsala, V., Vellore, R., and Kunchala, R.: Effectiveness of surface monitoring](#)
2085 [stations in representing regional CO₂ emissions over India, Clim. Res., 56, 121–129,](#)
2086 <https://doi.org/10.3354/cr01149>, 2013.

2087 [Tiwari, Y. K., Vellore, R. K., Ravi Kumar, K., Van Der Schoot, M., and Cho, C.-H.:](#)
2088 [Influence of monsoons on atmospheric CO₂ spatial variability and ground-based monitoring](#)
2089 [over India, Science of The Total Environment, 490, 570–578,](#)
2090 <https://doi.org/10.1016/j.scitotenv.2014.05.045>, 2014.

2091 [Vermote, E. and NOAA CDR Program: NOAA Climate Data Record \(CDR\) of AVHRR](#)
2092 [Normalized Difference Vegetation Index \(NDVI\), Version 5,](#)
2093 <https://doi.org/10.7289/V5ZG6QH9>, 2018.

2094 [Wada, A., Matsueda, H., Sawa, Y., Tsuboi, K., and Okubo, S.: Seasonal variation of](#)
2095 [enhancement ratios of trace gases observed over 10 years in the western North Pacific,](#)
2096 [Atmospheric Environment, 45, 2129–2137, https://doi.org/10.1016/j.atmosenv.2011.01.043,](#)
2097 [2011.](#)

2098 [Wang, G., Huang, J., Guo, W., Zuo, J., Wang, J., Bi, J., Huang, Z., and Shi, J.: Observation](#)
2099 [analysis of land-atmosphere interactions over the Loess Plateau of northwest China, Journal](#)
2100 [of Geophysical Research: Atmospheres, 115, https://doi.org/10.1029/2009JD013372, 2010.](#)

2101 [Wang, Z., Schaaf, C. B., Sun, Q., Shuai, Y., and Román, M. O.: Capturing rapid land surface](#)
2102 [dynamics with Collection V006 MODIS BRDF/NBAR/Albedo \(MCD43\) products, Remote](#)
2103 [Sensing of Environment, 207, 50–64, https://doi.org/10.1016/j.rse.2018.02.001, 2018.](#)

2104 [Watanabe, S., Miura, H., Sekiguchi, M., Nagashima, T., Sudo, K., Emori, S., and Kawamiya,](#)
2105 [M.: Development of an atmospheric general circulation model for integrated Earth system](#)
2106 [modeling on the Earth Simulator, Earth Simulator, 9, 27–35, 2008.](#)

2107 [Wigley, T. M. L. \(1983\). The pre-industrial carbon dioxide level. Climatic change, 5\(4\), 315-](#)
2108 [320.](#)

2109 [Worthy, D. E. J., Chan, E., Ishizawa, M., Chan, D., Poss, C., Dlugokencky, E. J., Maksyutov,](#)
2110 [S., and Levin, I.: Decreasing anthropogenic methane emissions in Europe and Siberia inferred](#)
2111 [from continuous carbon dioxide and methane observations at Alert, Canada, Journal of](#)
2112 [Geophysical Research: Atmospheres, 114, https://doi.org/10.1029/2008JD011239, 2009.](#)

2113 [Xiao, Y., Jacob, D. J., Wang, J. S., Logan, J. A., Palmer, P. I., Suntharalingam, P., Yantosca,](#)
2114 [R. M., Sachse, G. W., Blake, D. R., and Streets, D. G.: Constraints on Asian and European](#)
2115 [sources of methane from CH₄-C₂H₆-CO correlations in Asian outflow, J. Geophys. Res.,](#)
2116 [109, 2003JD004475, https://doi.org/10.1029/2003JD004475, 2004.](#)

2117 [Xiong, X., Houweling, S., Wei, J., Maddy, E., Sun, F., and Barnett, C.: Methane plume over](#)
2118 [south Asia during the monsoon season: satellite observation and model simulation,](#)
2119 [Atmospheric Chemistry and Physics, 9, 783–794, https://doi.org/10.5194/acp-9-783-2009,](#)
2120 [2009.](#)

2|21 [Yoro, K. O. and Daramola, M. O.: CO2 emission sources, greenhouse gases, and the global](#)
2|22 [warming effect, in: Advances in Carbon Capture, Elsevier, 3–28,](#)
2|23 <https://doi.org/10.1016/B978-0-12-819657-1.00001-3>, 2020.

2|24 [Yuan, Y., Ries, L., Petermeier, H., Steinbacher, M., Gómez-Peláez, A. J., Leuenberger, M.](#)
2|25 [C., Schumacher, M., Trickl, T., Couret, C., Meinhardt, F., and Menzel, A.: Adaptive selection](#)
2|26 [of diurnal minimum variation: a statistical strategy to obtain representative atmospheric CO₂](#)
2|27 [data and its application to European elevated mountain stations, Atmospheric Measurement](#)
2|28 [Techniques, 11, 1501–1514, https://doi.org/10.5194/amt-11-1501-2018](#), 2018.

2|29 [Zhang, H. F., Chen, B. Z., van der Laan-Luijk, I. T., Machida, T., Matsueda, H., Sawa, Y.,](#)
2|30 [Fukuyama, Y., Langenfelds, R., van der Schoot, M., Xu, G., Yan, J. W., Cheng, M. L., Zhou,](#)
2|31 [L. X., Tans, P. P., and Peters, W.: Estimating Asian terrestrial carbon fluxes from](#)
2|32 [CONTRAIL aircraft and surface CO₂ observations for the period 2006–2010,](#)
2|33 [Atmospheric Chemistry and Physics, 14, 5807–5824, https://doi.org/10.5194/acp-14-5807-](#)
2|34 [2014](#), 2014.

2|35 [Zhang, X., Nakazawa, T., Ishizawa, M., Aoki, S., Nakaoka, S.-I., Sugawara, S., Maksyutov,](#)
2|36 [S., Saeki, T., and Hayasaka, T.: Temporal variations of atmospheric carbon dioxide in the](#)
2|37 [southernmost part of Japan, Tellus B: Chemical and Physical Meteorology, 59, 654–663,](#)
2|38 <https://doi.org/10.1111/j.1600-0889.2007.00288.x>, 2007.

2|39

Formatted: Font colour: Black

Formatted: Normal, Space After: 12 pt, Border: Top: (No border), Bottom: (No border), Left: (No border), Right: (No border), Between : (No border)

Page 1: [1] Style Definition	Vimal Jose Vazhathara	13/03/2026 20:19:00
Revision: Font: (Default) Times New Roman, 12 pt,		
Page 1: [2] Style Definition	Vimal Jose Vazhathara	13/03/2026 20:19:00
Heading 6		
Page 1: [3] Style Definition	Vimal Jose Vazhathara	13/03/2026 20:19:00
Heading 5		
Page 1: [4] Style Definition	Vimal Jose Vazhathara	13/03/2026 20:19:00
Heading 4		
Page 1: [5] Style Definition	Vimal Jose Vazhathara	13/03/2026 20:19:00
Heading 3		
Page 1: [6] Style Definition	Vimal Jose Vazhathara	13/03/2026 20:19:00
Heading 2		
Page 1: [7] Style Definition	Vimal Jose Vazhathara	13/03/2026 20:19:00
Heading 1		
Page 1: [8] Style Definition	Vimal Jose Vazhathara	13/03/2026 20:19:00
Normal		
Page 1: [9] Formatted	Vimal Jose Vazhathara	13/03/2026 20:19:00
Font colour: Black		
Page 1: [10] Formatted	Vimal Jose Vazhathara	13/03/2026 20:19:00
Font colour: Black		
Page 1: [11] Formatted	Vimal Jose Vazhathara	13/03/2026 20:19:00
Font colour: Black		
Page 1: [12] Formatted	Vimal Jose Vazhathara	13/03/2026 20:19:00
Font colour: Black		
Page 1: [13] Formatted	Vimal Jose Vazhathara	13/03/2026 20:19:00
Font colour: Black		
Page 1: [14] Formatted	Vimal Jose Vazhathara	13/03/2026 20:19:00
Font colour: Black		
Page 1: [15] Formatted	Vimal Jose Vazhathara	13/03/2026 20:19:00
Font colour: Black		
Page 1: [16] Formatted	Vimal Jose Vazhathara	13/03/2026 20:19:00
Font colour: Black		
Page 1: [17] Formatted	Vimal Jose Vazhathara	13/03/2026 20:19:00
Font colour: Black		
Page 1: [18] Formatted	Vimal Jose Vazhathara	13/03/2026 20:19:00
Font colour: Black		
Page 1: [19] Formatted	Vimal Jose Vazhathara	13/03/2026 20:19:00
Font colour: Black		
Page 1: [20] Formatted	Vimal Jose Vazhathara	13/03/2026 20:19:00
Font colour: Black		

Page 1: [21] Formatted	Vimal Jose Vazhathara	13/03/2026 20:19:00
------------------------	-----------------------	---------------------

Font colour: Black

Page 1: [22] Formatted	Vimal Jose Vazhathara	13/03/2026 20:19:00
------------------------	-----------------------	---------------------

Font colour: Black

Page 1: [23] Formatted	Vimal Jose Vazhathara	13/03/2026 20:19:00
------------------------	-----------------------	---------------------

Font colour: Black

Page 1: [24] Formatted	Vimal Jose Vazhathara	13/03/2026 20:19:00
------------------------	-----------------------	---------------------

Font colour: Black

Page 1: [25] Formatted	Vimal Jose Vazhathara	13/03/2026 20:19:00
------------------------	-----------------------	---------------------

Font colour: Black

Page 1: [26] Formatted	Vimal Jose Vazhathara	13/03/2026 20:19:00
------------------------	-----------------------	---------------------

Font colour: Black

Page 1: [27] Formatted	Vimal Jose Vazhathara	13/03/2026 20:19:00
------------------------	-----------------------	---------------------

Font colour: Black

Page 1: [28] Formatted	Vimal Jose Vazhathara	13/03/2026 20:19:00
------------------------	-----------------------	---------------------

Font colour: Black

Page 1: [29] Formatted	Vimal Jose Vazhathara	13/03/2026 20:19:00
------------------------	-----------------------	---------------------

Font colour: Black

Page 9: [30] Deleted	Vimal Jose Vazhathara	13/03/2026 20:19:00
----------------------	-----------------------	---------------------

Page 9: [31] Deleted	Vimal Jose Vazhathara	13/03/2026 20:19:00
----------------------	-----------------------	---------------------

Page 14: [32] Deleted	Vimal Jose Vazhathara	13/03/2026 20:19:00
-----------------------	-----------------------	---------------------

Page 15: [33] Deleted	Vimal Jose Vazhathara	13/03/2026 20:19:00
-----------------------	-----------------------	---------------------

Page 15: [34] Deleted	Vimal Jose Vazhathara	13/03/2026 20:19:00
-----------------------	-----------------------	---------------------

Page 15: [35] Deleted	Vimal Jose Vazhathara	13/03/2026 20:19:00
-----------------------	-----------------------	---------------------

Page 15: [36] Deleted	Vimal Jose Vazhathara	13/03/2026 20:19:00
-----------------------	-----------------------	---------------------

Page 15: [37] Deleted	Vimal Jose Vazhathara	13/03/2026 20:19:00
-----------------------	-----------------------	---------------------

Page 16: [38] Deleted	Vimal Jose Vazhathara	13/03/2026 20:19:00
-----------------------	-----------------------	---------------------

Page 16: [39] Deleted	Vimal Jose Vazhathara	13/03/2026 20:19:00
-----------------------	-----------------------	---------------------

Page 16: [40] Deleted	Vimal Jose Vazhathara	13/03/2026 20:19:00
-----------------------	-----------------------	---------------------

Page 19: [41] Deleted **Vimal Jose Vazhathara** **13/03/2026 20:19:00**

▼

Page 19: [42] Deleted **Vimal Jose Vazhathara** **13/03/2026 20:19:00**

▼

Page 21: [43] Deleted **Vimal Jose Vazhathara** **13/03/2026 20:19:00**

▼

Page 21: [44] Deleted **Vimal Jose Vazhathara** **13/03/2026 20:19:00**

▼

Page 21: [45] Deleted **Vimal Jose Vazhathara** **13/03/2026 20:19:00**

▼

Page 21: [46] Deleted **Vimal Jose Vazhathara** **13/03/2026 20:19:00**

▼

Page 21: [47] Deleted **Vimal Jose Vazhathara** **13/03/2026 20:19:00**

▼

Page 21: [48] Deleted **Vimal Jose Vazhathara** **13/03/2026 20:19:00**

▼

Page 29: [49] Deleted **Vimal Jose Vazhathara** **13/03/2026 20:19:00**

▼